iScience

CellPress
OPEN ACCESS

Article

Porcine reproductive and respiratory syndrome virus upregulates SMPDL3B to promote viral replication by modulating lipid metabolism

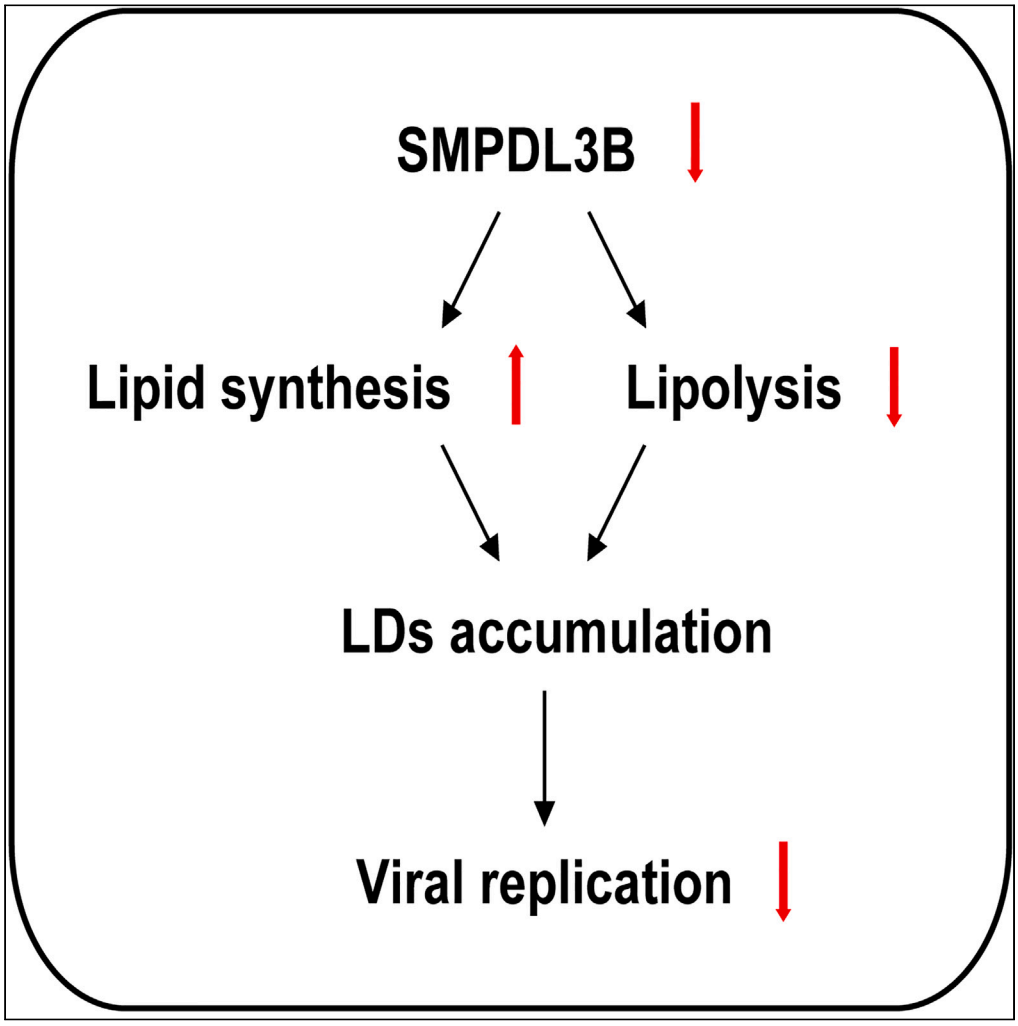

Huan-Huan Shen, Qin Zhao, Yi-Ping Wen, ..., San-Jie Cao, Lei Zeng, Qi-Gui Yan

zenglei2021918@163.com (L.Z.)
huanhshen@126.com (Q.-G.Y.)

Highlights

SMPDL3B was revealed as a host factor in PRRSV infection

SMPDL3B deficiency restricts the attachment, entry, replication, and secretion of PRRSV

SMPDL3B promotes PRRSV replication by modulating lipid metabolism

Shen et al., iScience 26, 107450
August 18, 2023
https://doi.org/10.1016/j.isci.2023.107450

iScience

CellPress
OPEN ACCESS

Article

Porcine reproductive and respiratory syndrome virus upregulates SMPDL3B to promote viral replication by modulating lipid metabolism

Huan-Huan Shen,[1,3] Qin Zhao,[1] Yi-Ping Wen,[1] Rui Wu,[1] Sen-Yan Du,[1] Xiao-Bo Huang,[1] Xin-Tian Wen,[1] San-Jie Cao,[1] Lei Zeng,[2,*] and Qi-Gui Yan[1,*]

SUMMARY

Porcine reproductive and respiratory syndrome virus (PRRSV) poses a severe threat to the health of pigs globally. Host factors play a critical role in PRRSV replication. Using PRRSV as a model for genome-scale CRISPR knockout (KO) screening, we identified a host factor critical to PRRSV infection: sphingomyelin phosphodiesterase acid-like 3B (SMPDL3B). Our findings show that SMPDL3B restricted PRRSV attachment, entry, replication, and secretion and that its depletion significantly inhibited PRRSV proliferation, indicating that SMPDL3B plays a positive role in PRRSV replication. Our data also show that SMPDL3B deficiency resulted in an accumulation of intracellular lipid droplets (LDs). The expression level of key genes (ACC, SCD-1, and FASN) involved in lipogenesis was increased, whereas the fundamental lipolysis gene, ATGL, was inhibited when SMPDL3B was knocked down. Overall, our findings suggest that SMPDL3B deficiency can effectively inhibit viral infection through the modulation of lipid metabolism.

INTRODUCTION

Porcine reproductive and respiratory syndrome (PRRS) is a highly contagious viral disease that affects pig.[1] PRRS is characterized by reproductive disorders in sows and respiratory diseases in pigs, especially piglets. Reproductive disorders in sows manifest as premature delivery, abortion, stillbirth, mummified fetuses, and weak litters.[2] Respiratory symptoms include cough, sneezing, and dyspnea.[3–6] PRRS virus (PRRSV) is a member of the arteriviridae family (Nidovirales) and is an enveloped, single-stranded RNA virus.[7] PRRSV can be divided into two types based on antigenicity, genome, and pathogenicity: European type and American type (also known as type 1 and type 2).[4,8,9] PRRSV primarily infects pulmonary alveolar macrophages (PAMs) *in vivo* due to its highly restricted cellular tropism.[10,11] The host factor, CD163, is essential for PRRSV replication.[12–14] While vaccine protection is currently the primary strategy for PRRSV defense, its efficacy is limited.[15]

Sphingomyelin phosphodiesterase acid-like 3B (SMPDL3B) is an enzyme belonging to the sphingomyelinase family known to play a critical role in the breakdown of sphingomyelin.[16,17] Sphingomyelin phosphodiesterase 1/acid sphingomyelinase is involved in the conversion of sphingomyelin to ceramide and phosphorylcholine.[18,19] Ceramide is known to regulate cellular responses, including growth arrest, senescence, apoptosis, and, more recently, autophagy.[20–22] It has been suggested that SMPDL3B may also be involved in these cellular activities, and recent studies have confirmed that SMPDL3B promotes cellular growth, invasion, and migration.[23] As a glycosylphosphatidylinositol (GPI)-anchored lipid raft SMPD, it comprises an N-terminal signal peptide (amino acid [aa] 1–18), a central metal phosphodiesterase domain (aa 23–323), and a C-terminal GPI membrane anchor.[24] SMPDL3B plays a key role in multiple essential cellular processes. A defect in SMPDL3B has been shown to partially restore cell survival and confer radioprotection,[25] and its defects affect Toll-like receptor (TLR)-mediated innate immunity in macrophages.[26] Mechanistically, SIRT1 regulates the transcription of SMPDL3B through c-Myc, thereby regulating sphingomyelin metabolism.[26] Recent studies have further demonstrated the relationship between SMPDL3B and lipid metabolism.[26,27] The latest research indicates that lipid metabolism has an effect on PRRSV replication.[28] This suggests a crucial role for lipid metabolism in PRRSV replication; however, little is known about the effect of SMPDL3B on PRRSV replication through lipid metabolism.

[1]College of Veterinary Medicine, Sichuan Agricultural University, Chengdu 610000, Sichuan Province, China

[2]College of Veterinary Medicine, Henan Agricultural University, Zhengzhou 450046, Henan Province, China

[3]Lead contact

*Correspondence: zenglei2021918@163.com (L.Z.), huanhshen@126.com (Q.-G.Y.)

https://doi.org/10.1016/j.isci.2023.107450

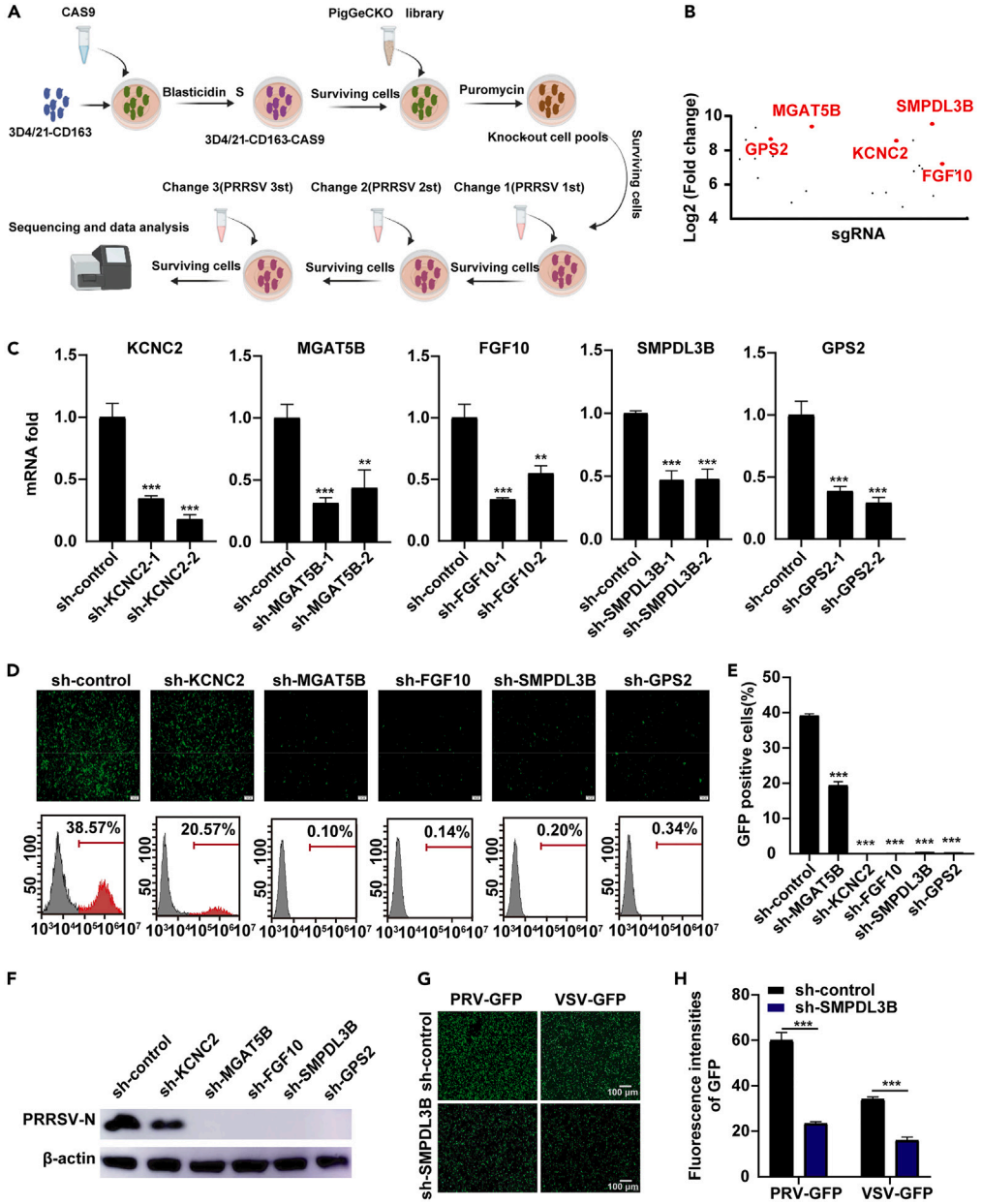

Figure 1. Genome-wide CRISPR screening was used to identify genes associated with PRRSV replication

(A) PigGeCKO library was used to identify the PRRSV host factors in pig cells. 3D4/21-CD163 cells were transformed and screened with puromycin (45 μg/μL). Transformed 3D4/21-CD163-Cas9 cells were challenged with PRRSV at an MOI = 0.01. Surviving cells from each round of viral challenge were isolated, amplified by PCR and sgRNA sequenced to identify the genes associated with PRRSV replication.

(B) The enrichment of sgRNA. Enrichment analysis of high-ranking sgRNA from panel A.

(C) The knockdown efficiency of KCNC2, MGAT5B, FGF10, GPS2, and SMPDL3B was detected by RT-qPCR. RNA was extracted from the cells and values were normalized to the mRNA levels of β-actin (ACTB). The data represent the means +/− standard errors of the means from three independent experiments. **$p < 0.01$, ***$p < 0.001$ (by an unpaired two-tailed *t*-test). The data represent the means +/− standard errors of the means from three independent experiments.

(D) Functional verification of candidate host factors. Fluorescent microscopy and FACS analysis of PRV-GFP (MOI = 10) proliferation in 3D4/21-CD163 and deficient cells for 36 h. Scale bar: 400 μm.

(E) GFP-positive cells from panel D.

(F) The levels of PRRSV-N protein expression were analyzed by immunoblotting in knockdown cells. Cells were infected with PRRSV-JXA1-R at an MOI of 0.1. Antibodies used are indicated on the left.

Figure 1. *Continued*
(G) Functional verification of SMPDL3B. Fluorescent microscopy analysis of PRV-GFP or VSV-GFP (MOI = 10) proliferation in sh-SMPDL3B stably expressed cells for 36 h. Scale bar: 400 μm.
(H) Fluorescence intensities of GFP from panel G.

Lipid metabolism comprises two distinct processes: fatty acid β-oxidation and lipid synthesis. Key lipogenic genes, such as acetyl-CoA carboxylase 1 (ACC1), fatty acid synthase (FASN), and stearoyl-CoA desaturase-1 (SCD-1),[29] and key lipolysis genes including triglyceride lipase (ATGL), hormone-sensitive lipase (HSL), and monoglyceride lipase (MGL)[30] are involved in these processes. Lipid droplets (LDs) play a crucial role in various stages of the viral life cycle, including attachment, entry, replication, assembly, and secretion.[31,32] LDs facilitate the replication of PRRSV by downregulating the expression of N-myc downstream-regulated gene 1.[28] Additionally, lipid rafts are known to be involved in many vital intracellular biochemical processes and play a significant role in PRRSV infection.[33] Furthermore, fatty acids, essential lipids, regulate PRRSV infection. Cholesterol 25-hydroxylase, another vital lipid, inhibits PRRSV replication.[34]

In this study, genome-scale CRISPR screening identified the host factors associated with PRRSV infection. SMPDL3B was identified as an essential candidate host factor for PRRSV replication. We demonstrated that a deficiency in SMPDL3B inhibited PRRSV replication, whereas SMPDL3B overexpression promoted its replication. Moreover, SMPDL3B deficiency inhibited PRRSV attachment, entry, replication, assembly, and secretion. SMPDL3B deficiency increased cellular LDs by promoting lipid synthesis and inhibiting lipid lipolysis. Intriguingly, SMPDL3B deficiency also inhibited the replication of vesicular stomatitis virus (VSV) and pseudorabies virus (PRV).

RESULTS

Genome-scale CRISPR screening identified host factors associated with PRRSV infection

To identify the host factors involved in PRRSV replication, we generated a collection of porcine genome-scale CRISPR-Cas9 knockout (PigGeCKO) cells on a PAM background and conducted genome-wide loss-of-function genetic screening. Prior to screening, we isolated and identified nine strains of PRRSV, all of which were found to be HP-PRRSV. We examined PRRSV-induced cell death following infection at various multiplicity of infection (MOI) values (0.001, 0.01, 0.1, and 1) and identified the optimal titer for PRRSV-induced cell death in PAM cells (MOI = 0.01). We then performed three rounds of screening to identify predisposing factors that regulate PRRSV-induced host cell death. The overall PigGeCKO screening strategy is shown in Figure 1A. The number of sgRNA copies theoretically indicates that the gene knockout confers strong resistance to PRRSV-induced 3D4/21-CD163 cell death without affecting cell growth. Among the positive selection CRISPR screening, the sgRNA enrichment result shows that SMPDL3B is the top enriched gene (Figure 1B). To assess the impact of highly enriched genes on PRRSV replication, cells were infected with PRRSV-GFP for 36 h (MOI = 10). Our results demonstrated that five candidate genes can be knocked down and the knocked-down cells can significantly inhibit the replication of PRRSV (Figures 1C–1E), Oligonucleotides were shown in Table 1. Surprisingly, we observed that a knockdown of SMPDL3B also inhibited PRRSV, VSV, and PRV replication (Figures 1F and 1G). Overall, our CRISPR-based screening strategy successfully identified multiple candidate host factors involved in PRRSV replication, and demonstrated that SMPDL3B was an essential host factor for PRRSV replication.

Expression profile of SMPDL3B

SMPDL3B is a lipid-modifying enzyme that converts sphingomyelin to ceramide in the cell membrane and regulates signaling by altering cell membrane fluidity. In this study, we aimed to determine the presence of SMPDL3B in different species by verifying the expression of the SMPDL3B protein in MARC-145, 293T/17, PAM, and L929 cells through western blot analysis (Figure 2A). Our results demonstrate that SMPDL3B was present in these cell lines, suggesting that it is widely distributed among different species.

PRRSV primarily infects the lung, which is the main phagocytic tissue of pigs. To investigate the level of SMPDL3B mRNA expression in different pig tissues, we employed semiquantitative RT-PCR (RT-qPCR). The analysis revealed that the white adipose tissue exhibited the highest level of SMPDL3B mRNA (Figure 2B), Oligonucleotides were shown in Table 2. This finding suggests that SMPDL3B may be associated with lipogenesis and lipolysis. The lung tissue of the pigs exhibited the second-highest level of SMPDL3B

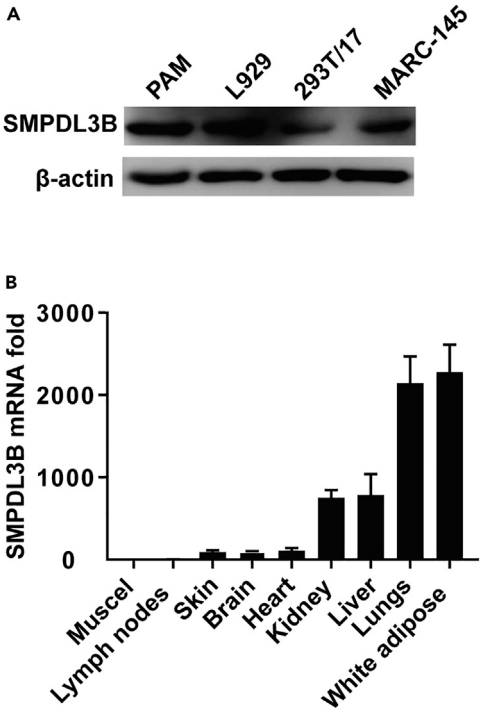

Figure 2. Analysis of SMPDL3B expression

(A) Immunoblot analysis of SMPDL3B expression in MARC-145, 293T/17, PAM, and L929 cells. The antibodies used are indicated on the left.

(B) RNA was extracted from porcine tissues, and the values were normalized to the level of β-actin (ACTB) mRNA expression. The relative amount of SMPDL3B mRNA was compared to that in the muscle. The data represent the means +/− standard errors of the means from three independent experiments.

mRNA (Figure 2B), which may explain why PRRSV is more likely to infect the lungs and why the viral load is higher in the lungs compared to that in other pig tissues and organs.[35]

PRRSV infection upregulates SMPDL3B expression

To investigate the impact of PRRSV infection on SMPDL3B expression, primary PAM and MARC-145 cells were infected with HP-PRRSV and LP-PRRSV and treated for different time periods. HP-PRRSV infection of MARC-145 cells led to a gradual increase in the level of SMPDL3B mRNA (Figure 3A), whereas HP-PRRSV infection of PAM cells resulted in a similar increase in SMPDL3B mRNA expression (Figure 3B), Oligonucleotides were shown in Table 2. Using a SMPDL3B-specific antibody, the level of SMPDL3B protein expression was detected, revealing a gradual increase, consistent with the SMPDL3B mRNA results (Figure 3C). LP-PRRSV was also inoculated into PAM and MARC-145 cells at different time points, leading to a gradual increase in the level of SMPDL3B mRNA and protein expression compared to the blank control group (Figures 3D–3F), Oligonucleotides were shown in Table 2. Overall, the results indicate that both HP-PRRSV and LP-PRRSV infection of PAM and MARC-145 cells could promote an increase in the level of SMPDL3B mRNA and protein expression. This phenomenon was also confirmed by immunofluorescence using confocal microscopy, which revealed that the level of SMPDL3B protein expression in PRRSV-positive cells (Figure 3G, white dotted line) was significantly increased compared to adjacent PRRSV-negative cells (Figure 3G, asterisks), albeit this was not visible to the naked eye. These results are consistent with previous studies that demonstrated that PRRSV infection could increase the level of SMPDL3B mRNA and protein expression.

SMPDL3B knockdown reduces PRRSV replication

To investigate the impact of SMPDL3B on PRRSV replication and proliferation, lentivirus-mediated short hairpin RNAs were employed to stably knock down SMPDL3B expression. RT-qPCR analysis revealed a significant reduction in the level of SMPDL3B mRNA expression in the Stable Knockout Cell Line compared to normal cells, indicating that the knockdown efficiency was successful (Figure 4A). The western blot results were consistent with RT-qPCR data, showing a marked decrease in SMPDL3B protein levels in the stably knocked down SMPDL3B cell line (Figure 4B). Furthermore, cell viability assessed using a cell counting kit demonstrated that the knockdown of SMPDL3B did not impact PAM cell growth within 96 h (Figure 4C).

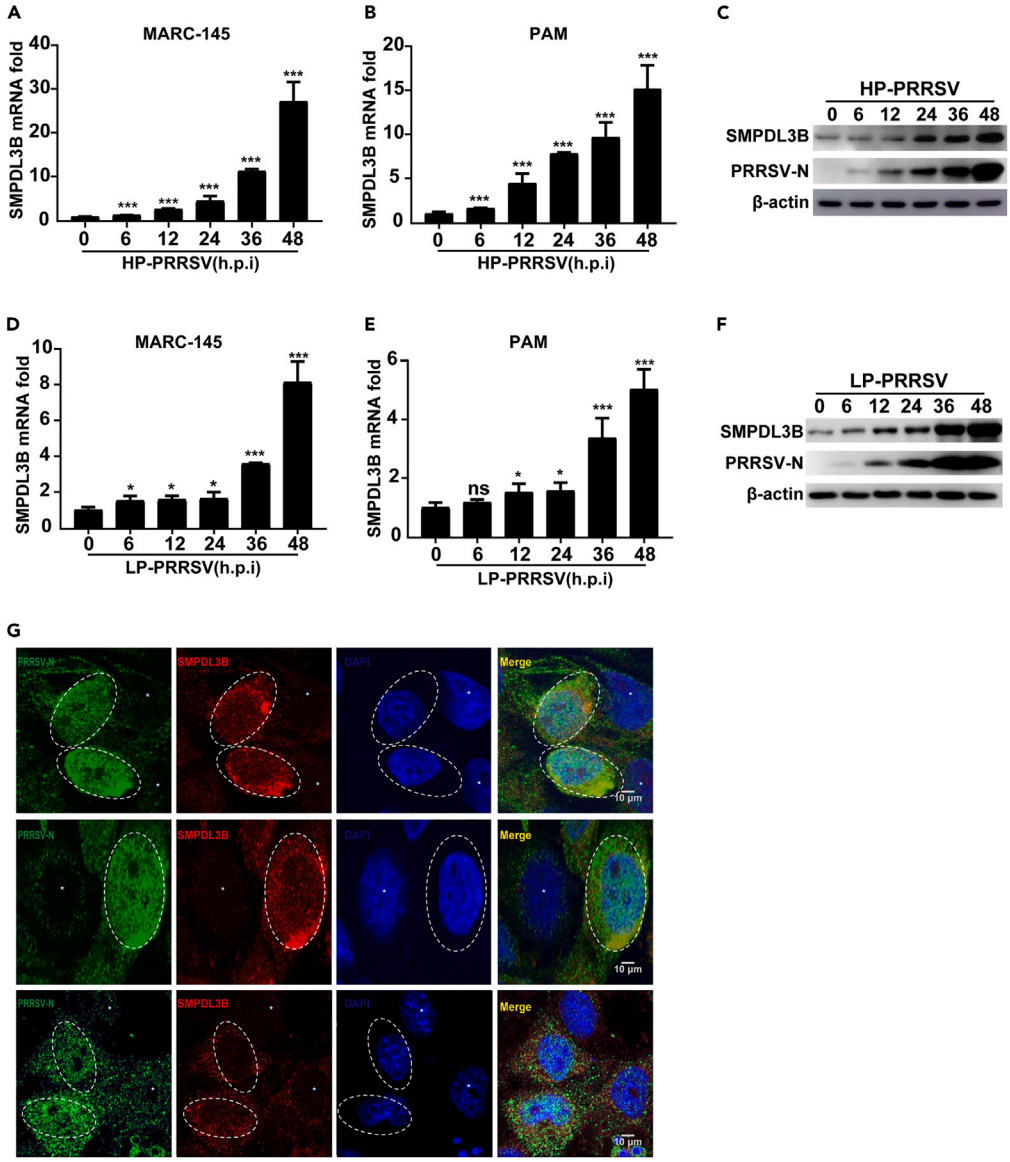

Figure 3. PRRSV infection increases the level of SMPDL3B mRNA and protein expression

(A) The level of SMPDL3B mRNA expression was detected in MARC-145 cells for the indicated time points by RT-qPCR. (MARC-145 cells infected with PRRSV-JXA1-R at an MOI of 0.1 for the indicated time points). RNA was extracted from MARC-145 cells at the indicated times. Values were normalized to the level of β-actin (ACTB) mRNA. Data represent means +/− standard errors of the means from three independent experiments. ***$p < 0.001$ (an unpaired two-tailed *t*-test).

(B) SMPDL3B mRNA levels were detected in PAM cells for the indicated time points by RT-qPCR. (PAM cells infected with PRRSV-JXA1-R at an MOI of 0.1 for the indicated time points). RNA was extracted from PAM cells at the indicated time points. ***$p < 0.001$ (an unpaired two-tailed *t*-test). ***$p < 0.001$ (an unpaired two-tailed *t*-test).

(C) The levels of SMPDL3B and PRRSV-N protein expression were analyzed by immunoblotting in PRRSV-infected PAM cells at different time points. Cells were infected with PRRSV-JXA1-R at an MOI of 0.1 and harvested at the indicated time points. Antibodies used are indicated on the left. (SMPDL3B: Rabbit anti-SMPDL3B antibody; PRRSV-N: Rabbit anti-PRRSV-N antibody; β-actin: Sheep anti-rabbit antibody).

(D) SMPDL3B mRNA levels were detected in MARC-145 cells for the indicated time points by RT-qPCR. Cells were infected with PRRSV-VR2332 at an MOI of 0.1 and RNA was extracted at the indicated time points. *$p < 0.05$, ***$p < 0.001$ (an unpaired two-tailed *t*-test).

Figure 3. *Continued*

(E) The expression of SMPDL3B mRNA was analyzed by RT-qPCR in PRRSV-infected PAM cells at different time points. Cells were infected with PRRSV-VR2332 at an MOI of 0.1 and RNA was extracted at the indicated times. ns, not significant *$p < 0.05$, ***$p < 0.001$ (an unpaired two-tailed *t*-test).

(F) The levels of SMPDL3B protein expression and PRRSV-N were analyzed by immunoblotting in PRRSV-infected PAM cells at different time points. Cells were infected with PRRSV-VR2332 at an MOI of 0.1 and harvested at the indicated time points. The used antibodies are indicated on the left (SMPDL3B: Rabbit anti-SMPDL3B antibody; PRRSV-N: Rabbit anti-PRRSV-N antibody; β-actin: Sheep anti-rabbit antibody).

(G) SMPDL3B staining was increased in PRRSV-infected cells. MARC-145 cells were infected with PRRSV-JXA1-R at an MOI of 0.01 for 48 h, fixed, and stained with antibodies against PRRSV-N (green) and SMPDL3B (red). Infected cells are highlighted by white dotted lines, and uninfected cells are indicated by asterisks.

To confirm the effect of a SMPDL3B deficiency on PRRSV replication, we infected 3D4/21-CD163 and SMPDL3B-deficient cells with HP-PRRSV for 48 h. RT-qPCR analysis of the isolated virus revealed that SMPDL3B deficiency significantly reduced the level of PRRSV-ORF7 compared to the control group (Figure 4D), indicating that a SMPDL3B deficiency can significantly inhibit PRRSV replication. SMPDL3B serves as an anti-inflammatory receptor, negatively regulating the innate immune response.[36] In our experiment, we validated that knocking down SMPDL3B can promote the expression of innate immune (Figures 4E–4H) (Oligonucleotides were shown in Table 2) due to the enhanced cytokine expression, which resulted in suppression of infection.[37] This may also be one of the reasons why PRRSV replication is suppressed. Western blot results further showed that the level of PRRSV-N protein expression in the SMPDL3B knockdown group was significantly lower than that in the control group (Figures 4I and 4J), supporting the notion that PRRSV replication was significantly inhibited in the SMPDL3B deficiency group. We measured the proliferation curve of PRRSV in 3D4/21-CD163 and SMPDL3B deficiency cells and found that the proliferation of PRRSV was significantly reduced in SMPDL3B-deficient cells (Figure 4K). The reduction in PRRSV production was confirmed by measuring the viral titer in SMPDL3B-deficient cells (Figure 4L). These data collectively suggest that SMPDL3B deficiency inhibits PRRSV replication in 3D4/21-CD163 cells. This being the case, would that happen in MARC-145 cells? As shown in Figures 4M and 4N, the level of SMPDL3B and PRRSV mRNA was significantly reduced in SMPDL3B-deficient MARC-145 cells sh-control cells, indicating that SMPDL3B deficiency inhibits PRRSV replication in MARC-145 cells. Western blot results further showed that the level of PRRSV-N protein expression in SMPDL3B-deficient MARC-145 cells was significantly lower (Figure 4O). There is no significant difference in the expression level of Smpdl3b mRNA in SMPDL3B-rescue cell and sh-control cells (Figure 4P). Western blot results were consistent with RT-qPCR data (Figure 4Q), suggesting that we performed a successful SMPDL3B rescue efficiency. There was no significant difference in the mRNA level of PRRSV in SMPDL3B-rescue cell and sh-control cells (Figure 4R); western blot results were consistent with RT-qPCR data (Figure 4S). These results suggested that SMPDL3B-rescue can restore the promoting effect of SMPDL3B on PRRSV replication (Figures 4P–4S), and the FACS analysis result of PRRSV-GFP in SMPDL3B-rescue cells or sh-control cells was consistent with this conclusion (Figure 4T). These data collectively suggest that SMPDL3B knockout inhibits PRRSV replication and that SMPDL3B plays a positive role in PRRSV replication.

SMPDL3B overexpression enhances PRRSV replication

The aforementioned results verified a positive regulatory role of SMPDL3B in PRRSV replication. To further confirm this role, we transfected PAM cells with an empty or varying amounts of FLAG-SMPDL3B for 24 h prior to PRRSV infection. The RT-qPCR and western blot analyses revealed that the increase in SMPDL3B levels significantly enhanced PRRSV mRNA and N protein levels (Figures 5A and 5B). The same phenomenon was observed in MARC-145 cells, where increasing levels of SMPDL3B led to a corresponding increase in PRRSV mRNA and N protein levels (Figures 5D and 5E). The increase in PRRSV production was confirmed by measuring the viral titer in SMPDL3B overexpression cells, which exhibited a dose-dependent effect (Figure 5G). This phenotype was also confirmed by fluorescence confocal microscopy, in which PRRSV replication in SMPDL3B overexpression cells (Figure 5H, white dotted lines) was significantly higher than that in the adjacent non-control cells (Figure 5H, arrowheads). These results strongly support a positive regulatory role of SMPDL3B in PRRSV replication.

SMPDL3B deficiency restricts the attachment, entry, replication, and secretion of PRRSV but not assembly

It has been previously established that SMPDL3B deficiency impedes PRRSV replication. Here, we investigated the impact of SMPDL3B deficiency on various stages of the PRRSV life cycle. Cells were transfected

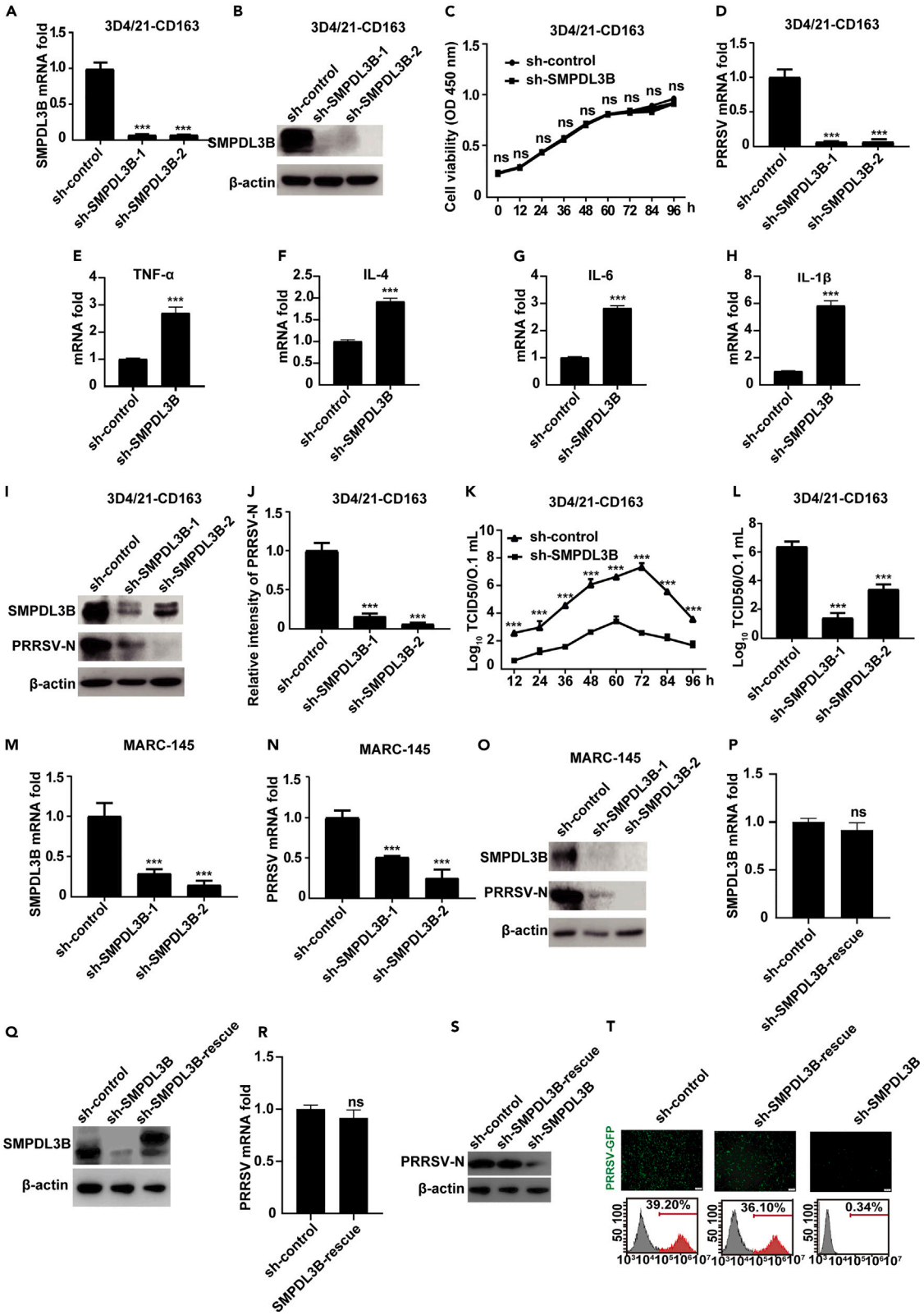
A
3D4/21-CD163
SMPDL3B mRNA fold
sh-control
sh-SMPDL3B-1
sh-SMPDL3B-2
B
3D4/21-CD163
SMPDL3B
β-actin
C
3D4/21-CD163
sh-control
sh-SMPDL3B
Cell viability (OD 450 nm)
h
D
3D4/21-CD163
PRRSV mRNA fold
E
TNF-α
mRNA fold
sh-SMPDL3B
F
IL-4
G
IL-6
H
IL-1β
I
3D4/21-CD163
PRRSV-N
J
3D4/21-CD163
Relative intensity of PRRSV-N
K
3D4/21-CD163
Log10 TCID50/0.1 mL
L
3D4/21-CD163
M
MARC-145
N
MARC-145
O
MARC-145
P
sh-SMPDL3B-rescue
ns
Q
R
S
T
PRRSV-GFP
39.20%
36.10%
0.34%

Figure 4. SMPDL3B knockdown inhibits PRRSV infection

(A) TNF-α mRNA levels were detected in the cells by RT-qPCR. Values were normalized to the level of β-actin mRNA (ACTB), and the data represent the means +/− standard errors of the means from three independent experiments. ***p < 0.001 (by an unpaired two-tailed *t*-test).

(B) IL-4 mRNA levels were detected in the cells by RT-qPCR. Values were normalized to the level of β-actin mRNA (ACTB), and the data represent the means +/− standard errors of the means from three independent experiments. ***p < 0.001 (by an unpaired two-tailed *t*-test).

(C) IL-6 mRNA levels were detected in the cells by RT-qPCR. Values were normalized to the level of β-actin mRNA (ACTB), and the data represent the means +/− standard errors of the means from three independent experiments. ***p < 0.001 (by an unpaired two-tailed *t*-test).

(D) IL-1β mRNA levels were detected in the cells by RT-qPCR. Values were normalized to the level of β-actin mRNA (ACTB), and the data represent the means +/− standard errors of the means from three independent experiments. ***p < 0.001 (by an unpaired two-tailed *t*-test).

(E) SMPDL3B mRNA levels in stably expressing sh-SMPDL3B or sh-control cells were detected by RT-qPCR. RNA was extracted from the cells and values were normalized to the level of β-actin mRNA (ACTB). The data represent the means +/− standard errors of the means from three independent experiments. ***p < 0.001 (by an unpaired two-tailed *t*-test).

(F) Immunoblot analysis of SMPDL3B expression in cells from panel A. The antibodies that were used are indicated on the left (SMPDL3B: Rabbit anti-SMPDL3B antibody; β-actin: Sheep anti-rabbit antibody).

(G) Proliferation of cells in stably expressing sh-SMPDL3B or sh-control 3D4/21-CD163 cells was determined by a CCK assay. OD, optical density; ns, not significant (by an unpaired two-tailed *t*-test).

(H) PRRSV mRNA levels were detected in the cells by RT-qPCR. (cells infected with PRRSV-JXA1-R at an MOI of 0.1 for 48 h). Values were normalized to the level of β-actin mRNA (ACTB), and the data represent the means +/− standard errors of the means from three independent experiments. ***p < 0.001 (by an unpaired two-tailed *t*-test).

(I) Immunoblot analysis of SMPODL3B expression in stably expressing sh-SMPDL3B or sh-control 3D4/21-CD163 cells. Antibodies that were used are indicated on the left (SMPDL3B: Rabbit anti-SMPDL3B antibody; PRRSV-N: Rabbit anti-PRRSV-N antibody; β-actin: Sheep anti-rabbit antibody).

(J) A semiquantitative densitometric analysis of PRRSV-N from panel E was performed using ImageJ software. The protein content was normalized to the corresponding β-actin content.

(K) Growth curve of PRRSV. The growth curve of PRRSV was determined in 3D4/21-CD163 cells stably expressing sh-SMPDL3B or sh-control, infected with PRRSV (MOI = 0.1) for the indicated time points. Virus was harvested with three freeze-thaw cycles and the viral titer was determined by a TCID50 assay. Values were normalized to the level of β-actin mRNA (ACTB). Data represent the means +/− standard errors of the means from three independent experiments. ***p < 0.001 Statistical significance was determined by an unpaired two-tailed *t*-test.

(L) Viral titers of PRRSV. 3D4/21-CD163 cells stably expressing sh-SMPDL3B or sh-control were infected with PRRSV-JXA1-R (MOI = 0.1) for 48 h. Virus was harvested with three freeze-thaw cycles and the viral titer was determined by a TCID50 assay. Values were normalized to the level of β-actin mRNA (ACTB). Data represent the means +/− standard errors of the means from three independent experiments. ***p < 0.001. Statistical significance was determined by an unpaired two-tailed *t*-test.

(M) SMPDL3B mRNA levels. The levels of SMPDL3B mRNA in stably expressing sh-SMPDL3B or sh-control cells were detected by RT-qPCR. RNA was extracted from sh-SMPDL3B and sh-control MARC-145 cells. Values were normalized to the levels of β-actin mRNA expression (ACTB). Data represent the means +/− standard errors of the means from three independent experiments. Statistical significance was determined by an unpaired two-tailed *t*-test ***p < 0.001.

(N) PRRSV mRNA levels. The levels of PRRSV mRNA were detected in cells stably expressing sh-SMPDL3B or sh-control MARC-145 cells infected with PRRSV-JXA1-R (MOI = 0.1) for 48 h using RT-qPCR. RNA was extracted from cells and values were normalized to the levels of β-actin mRNA expression (ACTB). Data represent the means +/− standard errors of the means from three independent experiments. Statistical significance was determined by an unpaired two-tailed *t*-test ***p < 0.001.

(O) Immunoblot analysis of SMPDL3B expression in cells from panel K was analyzed by immunoblotting. Antibodies used are indicated on the left (SMPDL3B: Rabbit anti-SMPDL3B antibody; PRRSV-N: Rabbit anti-PRRSV-N antibody; β-actin: Sheep anti-rabbit antibody).

(P) SMPDL3B mRNA Levels. The levels of SMPDL3B mRNA in SMPDL3B-rescue or sh-control cells were detected by RT-qPCR. Values were normalized to the levels of β-actin mRNA expression (ACTB). ns, not significant. Statistical significance was determined by an unpaired two-tailed *t*-test.

(Q) Immunoblot analysis of SMPDL3B expression in cells from panel L was analyzed by immunoblotting. Antibodies used are indicated on the left (SMPDL3B: Rabbit anti-SMPDL3B antibody; β-actin: Sheep anti-rabbit antibody.).

(R) PRRSV mRNA levels. The levels of PRRSV mRNA were detected in SMPDL3B-rescue or sh-control cells. Cells were infected with PRRSV-JXA1-R (MOI = 0.1) for 48 h using RT-qPCR. Statistical significance was determined by an unpaired two-tailed *t*-test. ns, not significant.

(S) Immunoblot analysis of PRRSV-N expression in SMPDL3B-rescue or sh-control cells. Antibodies used are indicated on the left (PRRSV-N: Rabbit anti-PRRSV-N antibody; β-actin: Sheep anti-rabbit antibody.).

(T) Replication of PRRSV-GFP in SMPDL3B-rescue or sh-control cells. Fluorescent microscopy and FACS analysis of PRRSV-GFP (MOI = 10) proliferation in 3D4/21-CD163 and deficient cells for 36 h. Scale bar: 400 μm.

with either empty sh-control (control group) or sh-SMPDL3B and subsequently incubated with a high multiplicity of infection (MOI = 10) of PRRSV on ice for 1 h. RT-qPCR was performed to detect the adsorbed PRRSV. RT-qPCR results showed that the level of PRRSV binding to SMPDL3B-deficient cells was significantly lower than that of the control group (Figure 6A). This phenomenon was further confirmed with immunofluorescence using confocal microscopy. Specifically, sh-SMPDL3B and sh-control cells were incubated with a PRRSV-N-specific antibody and the green fluorescence of PRRSV-N protein in SMPDL3B-deficient cells (Figure 6B white dotted line) was significantly lower than in the control cells (Figure 6B white dotted line). We used RT-qPCR to determine if SMPDL3B deficiency affected the internalization of PRRSV. Knockdown cells were incubated with PRRSV at 37°C for 1 h. The results showed that the level of viral entry into

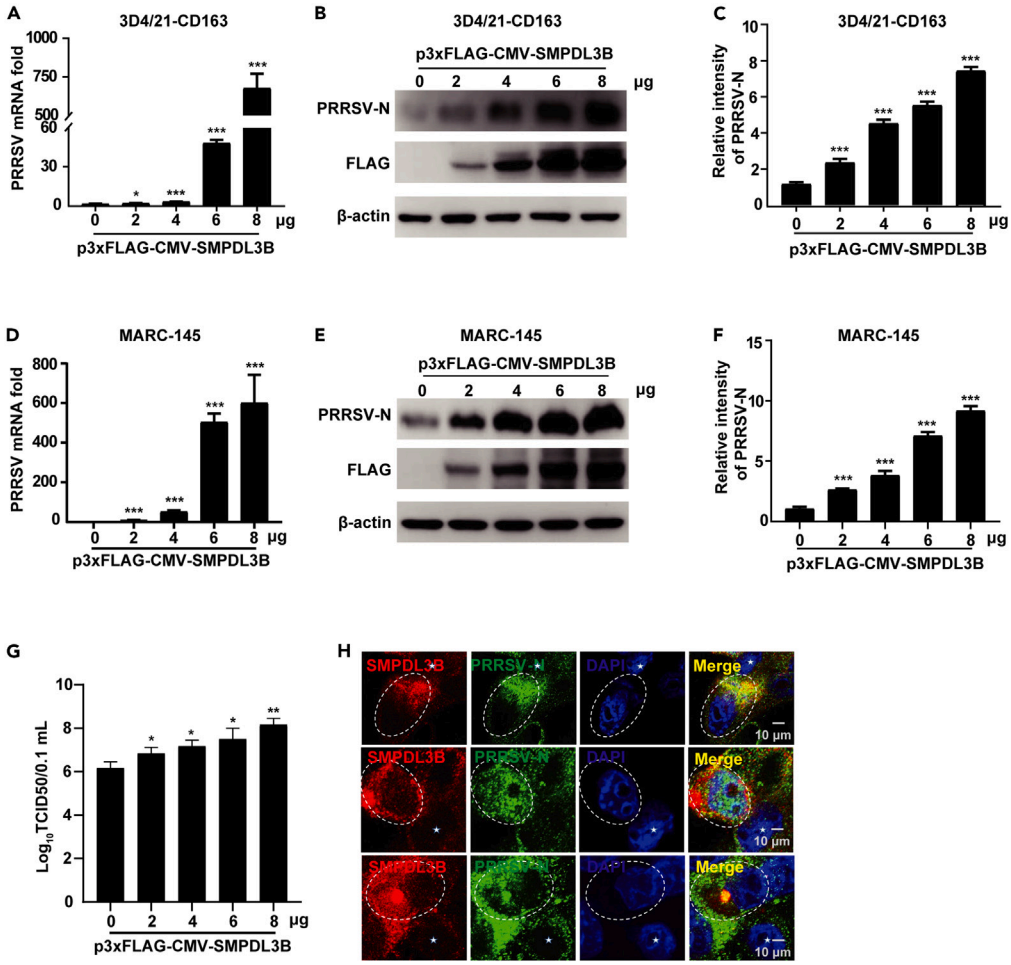

Figure 5. SMPDL3B overexpression increased PRRSV replication

(A) PRRSV mRNA levels were detected in cells by RT-qPCR. The cells were transfected with different amounts of p3xFlag-CMV-14-SMPDL3B plasmids for 24 h, followed by an infection with PRRSV (PRRSV-JXA1-R MOI = 0.1) for 48 h. RNA was extracted from cells, and the values were normalized to the level of β-actin (ACTB) mRNA expression. The data represent the means +/−standard errors of the means from three independent experiments. Statistical significance was determined using an unpaired two-tailed *t*-test with *p < 0.05 and ***p < 0.001.

(B) Immunoblot analysis of SMPDL3B expression in cells from panel A. Antibodies used in the experiments are indicated on the left (PRRSV-N: Rabbit anti-PRRSV-N antibody; FLAG: Rabbit anti-FLAG antibody; β-actin: Sheep anti-rabbit antibody).

(C) Semiquantitative densitometric analysis of PRRSV-N from panel B was performed using ImageJ software. Protein content was normalized to the corresponding β-actin content.

(D) PRRSV mRNA levels were detected in cells by RT-qPCR. MARC-145 cells transfected with different amounts of p3xFlag-CMV-14-SMPDL3B plasmids for 24 h, followed by infection with PRRSV (PRRSV-JXA1-R MOI = 0.1) for 48 h. RNA was extracted from cells, and the values were normalized to the level of β-actin (ACTB) mRNA. The data represent the means +/− standard errors of the means from three independent experiments. Statistical significance was determined using an unpaired two-tailed *t*-test. ***p < 0.001.

(E) Immunoblot analysis of SMPDL3B expression in the cells from panel F. Antibodies used are indicated on the left (PRRSV-N: Rabbit anti-PRRSV-N antibody; FLAG: Rabbit anti-FLAG antibody; β-actin: Sheep anti-rabbit antibody).

(F) Semiquantitative densitometric analysis of PRRSV-N from panel E was performed using ImageJ software. Protein content was normalized to the corresponding β-actin content.

(G) Viral Titers of PRRSV. 3D4/21-CD163 cells were transfected with various amounts of p3xFlag-CMV-14-SMPDL3B plasmids for 24 h followed by an infection with PRRSV-JXA1-R at an MOI of 0.1 for 48 h. The virus was harvested with three cycles of freezing and thawing, and the viral titer was determined using the TCID50 assay.

(H) Staining for PRRSV-N was increased in the overexpressing SMPDL3B cells. Cells were infected with PRRSV-JXA1-R at an MOI of 0.1 for 48 h, fixed, and then stained using antibodies against PRRSV-N (green) and SMPDL3B (red). Infected cells were highlighted with white dotted lines, and uninfected cells were indicated with asterisks.

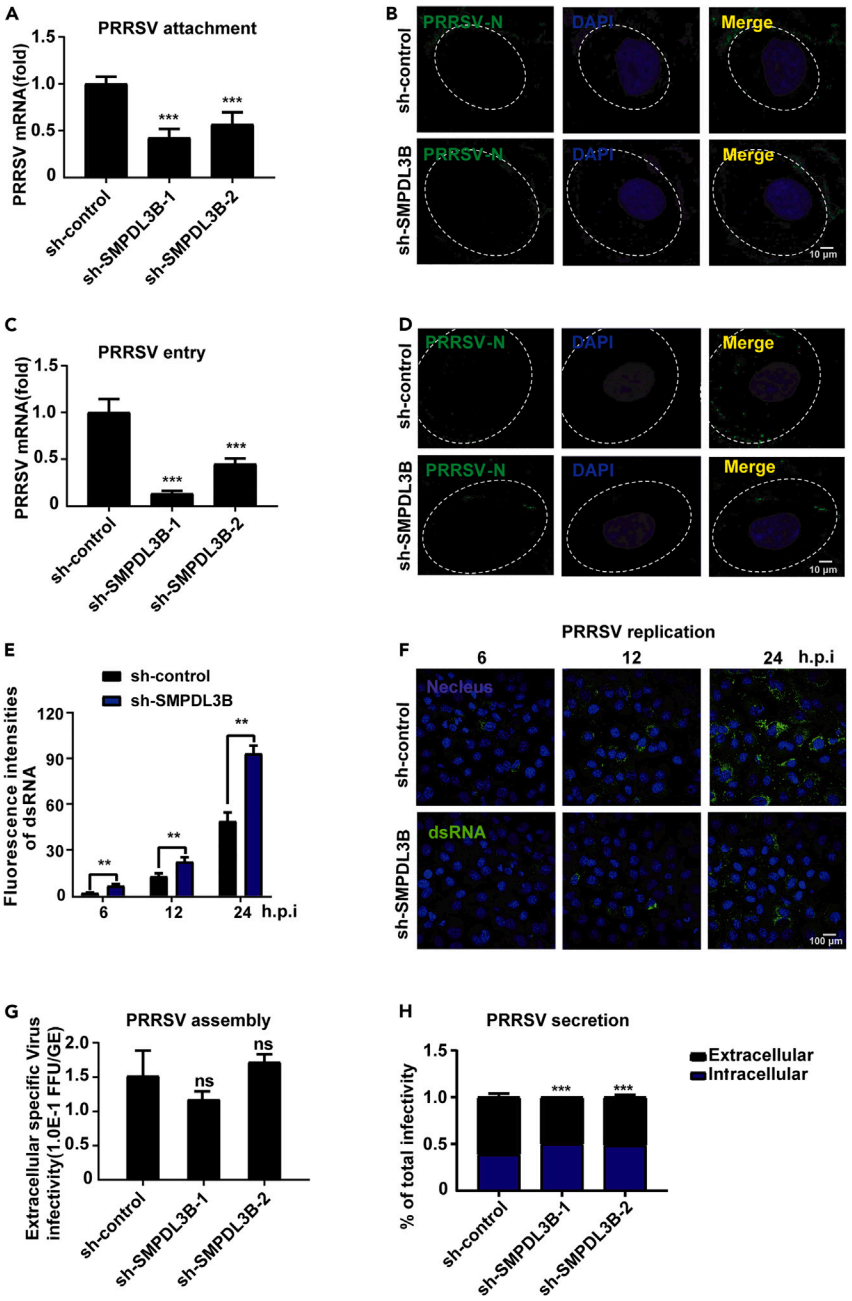

Figure 6. SMPDL3B restricts the attachment, entry, replication, and secretion of PRRSV, but not assembly

(A) RT-qPCR analysis was performed to determine the number of PRRSV particles on the surface of stably expressing sh-SMPDL3B or sh-control cells. The cells were incubated with PRRSV (MOI = 10) for 1 h on ice, and then washed three times with precooled PBS. RNA was extracted from the cells, and the values were normalized to the level of β-actin (ACTB) mRNA expression. The data represent the means +/− standard errors of the means from three independent experiments. Statistical analysis was performed using an unpaired two-tailed *t*-test, and ***$p < 0.001$ was considered significant.

(B) Immunofluorescence of PRRSV-N on the surface of sh-SMPDL3B or sh-control cells. The cells were incubated with PRRSV (MOI = 10) for 1 h on ice, and then washed three times with precooled PBS. The cells were fixed and stained with antibodies directed against PRRSV-N (green). Infected cells were highlighted by white dotted lines.

(C) RT-qPCR analysis of PRRSV numbers in stably expressing sh-SMPDL3B or sh-control cells. The cells were incubated with PRRSV (MOI = 10) for 1 h at 37°C and then washed twice with trypsin. RNA was extracted from the cells, and the values were normalized to the level of β-actin (ACTB) mRNA expression. The data represent the means +/− standard errors of

Figure 6. *Continued*

the means from three independent experiments. Statistical analysis was performed using an unpaired two-tailed *t*-test, and ***$p < 0.001$ was considered significant.

(D) Immunofluorescence of PRRSV-N in sh-SMPDL3B or sh-control cells. The cells were incubated with PRRSV (MOI = 10) for 1 h at 37°C and then washed twice with trypsin. The cells were fixed and stained with antibodies directed against PRRSV-N (green). Infected cells were highlighted by white dotted lines.

(E) Fluorescence intensities of dsRNA in panel F were quantified in cells containing PRRSV dsRNA.

(F) The immunofluorescence of ds-RNA in sh-SMPDL3B or sh-control cells. The cells were incubated with PRRSV (MOI = 10) for 1 h and cultured for the indicated time points. The cells were then fixed and stained with antibodies directed against dsRNA (green).

(G) The efficiency of viral assembly was determined by the ratio of the virus titer in the supernatant to the total PRRSV genome. The cells were incubated with PRRSV (MOI = 10) for 1 h and cultured for 24 h. The data represent the means +/− standard errors of the means from three independent experiments. Statistical analysis was performed using an unpaired two-tailed *t*-test, and ***$p < 0.001$ was considered significant.

(H) The efficiency of viral secretion was determined by the ratio of intra- and extracellular infectivity relative to total infectivity. The cells were incubated with PRRSV (MOI = 10) for 1 h and cultured for 24 h. The data represent the means +/− standard errors of the means from three independent experiments. Statistical analysis was performed using an unpaired two-tailed *t*-test, and ***$p < 0.001$ was considered significant.

SMPDL3B-deficient cells was significantly lower than that of the control group (Figure 6C). We also confirmed that SMPDL3B deficiency reduces PRRSV internalization with immunofluorescence using confocal microscopy (Figure 6D). To investigate the effect of SMPDL3B deficiency on PRRSV replication, PRRSV-infected cells were fixed and stained for double-stranded RNA (dsRNA) at 6, 12, or 24 h, as a marker of viral replication. The green fluorescence of the SMPDL3B-deficient group was significantly lower than that of the control group at 6, 12, and 24 h (10 random fields of view; $n > 100$ cells each) (Figures 6E and 6F). This indicated that SMPDL3B deficiency can significantly inhibit PRRSV replication. To further verify the impact of SMPDL3B on PRRSV assembly and release, the results confirmed that SMPDL3B deficiency inhibited the release of PRRSV but not viral assembly (Figures 6G and 6H). In summary, our results indicate that SMPDL3B deficiency inhibits the attachment, entry, replication, and secretion of PRRSV, but not its assembly.

SMPDL3B plays a key role in lipid synthesis and lipid lipolysis

We hypothesized that SMPDL3B may affect PRRSV replication through LDs. To test this hypothesis, we stained SMPDL3B-deficient cell lines with oil red O and BODIPY 493/503, as previously described by Qiu and Simon.[38] Under the microscope, we observed that the number of LDs was significantly increased in SMPDL3B-deficient cells compared to the control cells ($p < 0.0001$) (Figures 7A and 7B). Additionally, the fluorescence intensity of the SMPDL3B-deficient cells was over four times higher than that of the sh-control group ($p < 0.0001$) (Figures 7C and 7D). Therefore, we concluded that a SMPDL3B deficiency promotes LD accumulation. We speculated that the reason for the LD accumulation was due to the SMPDL3B deficiency affecting lipid synthesis or lipolysis. We found that the level of mRNA expression of the key genes involved in lipid synthesis, including fatty acid FASN, SCD1, and ACC1, was significantly higher in SMPDL3B-deficient cells than in the sh-control cells (Figure 7E), Oligonucleotides were shown in Table 2. Moreover, the mRNA levels of key lipolysis genes including ATGL, HSL, and MGL were significantly reduced (Figure 7F), Oligonucleotides were shown in Table 2. The results showed that a SMPDL3B deficiency promoted lipid synthesis and inhibits lipolysis (Figures 7E–7G). To further verify our conclusion, SMPDL3B-rescue cells were performed and stained with oil red O, as shown in (Figures 7H and 7I); the number of LDs per cell was significantly increased in SMPDL3B-rescue cells compared to the SMPDL3B-deficient cells ($p < 0.0001$). Thus, our results demonstrate that SMPDL3B plays a critical role in lipid synthesis and lipolysis.

DISCUSSION

PRRSV poses a severe threat to pig health worldwide. Additional studies are required to investigate the replication mechanisms of PRRSV, which can be conducive to the prevention and treatment of PRRSV, as well as the research and development of new drug targets. Host functional factors play an important role in viral replication. CRISPR-Cas9 genome editing technology is easier to operate, cheaper, more efficient, more accurate, and less off-target.[39–41] Moreover, it has also been successfully applied in a variety of organisms.[42,43] In a genome-scale CRISPR screening following three PRRSV challenges, SMPDL3B was identified as a functional factor. Currently, the known PRRSV functional factors include CD163 (cluster of differentiation 163),[12,44] heparin sulfate,[45]

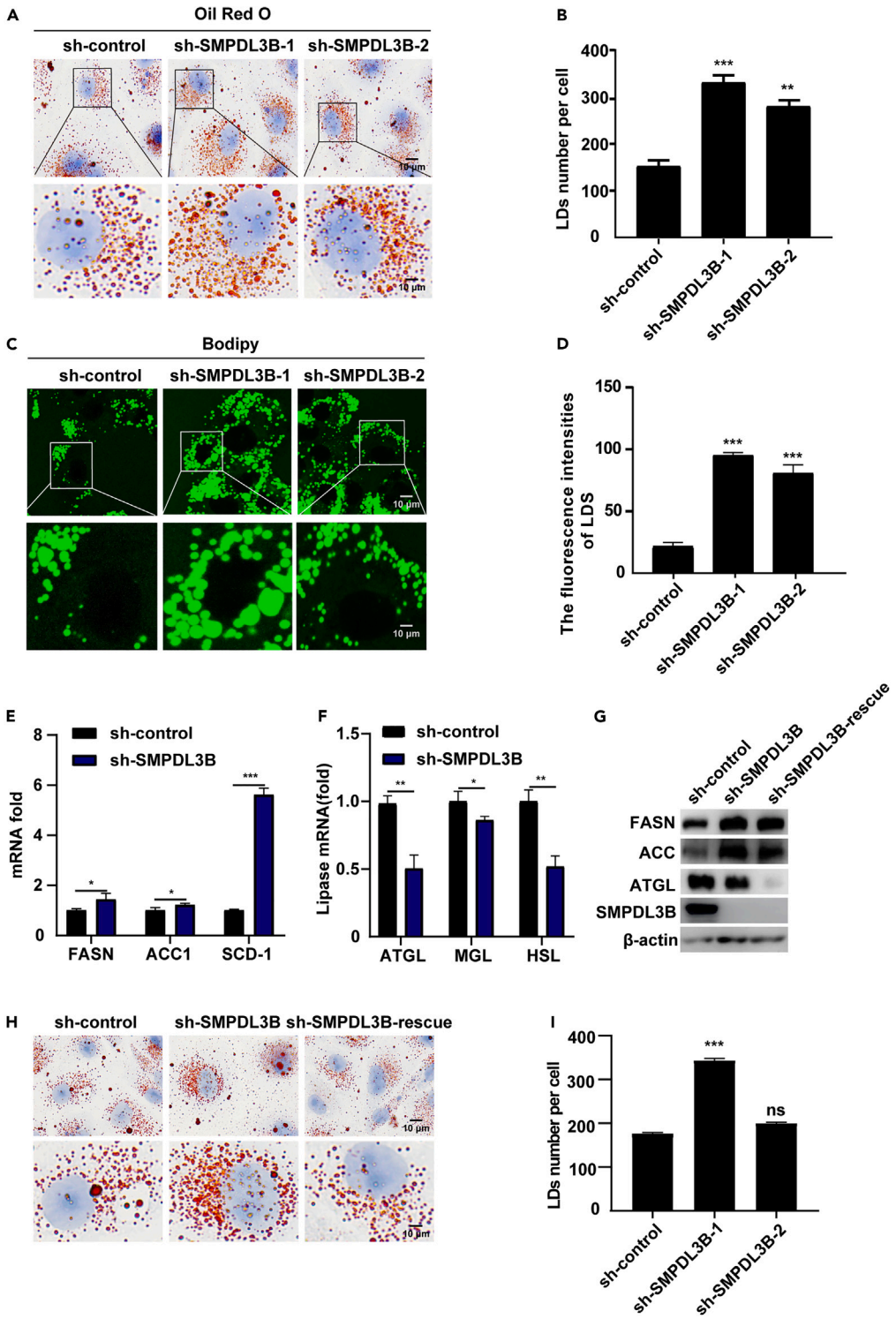

Figure 7. SMPDL3B plays a key role in lipid synthesis and lipid lipolysis

(A) Cells were stained with oil red O. Sh-SMPDL3B or sh-control cells were fixed with 4% paraformaldehyde, stained with oil red O, and counterstained with hematoxylin. The bottom image corresponds to the boxed region marked in the upper image. Each image is representative of three independent experiments.

Figure 7. *Continued*

(B) Number of lipid droplets (LDS) per cell. The number of LDS per cell was quantified in each image. At least 80 cells were counted. Data are representative of the means +/− standard errors of the means from three independent experiments. **p < 0.01; ***p < 0.001 (by an unpaired two-tailed *t*-test).

(C) Cells were stained with BODIPY 493/503. Sh-SMPDL3B or sh-control cells were fixed and stained with BODIPY. The bottom image corresponds to the boxed region marked in the upper image. Each image represents three independent experiments.

(D) The LDS fluorescence intensities. The fluorescence intensities of LDS were analyzed using ImageJ software. Data are representative of the means +/− standard errors of the means of three independent experiments. ***p < 0.001 (by an unpaired two-tailed *t*-test).

(E) Levels of ACC1, FASN, and SCD were detected by RT-qPCR. RNA was extracted from stably expressing sh-SMPDL3B or sh-control cells. Values were normalized to the level of β-actin (ACTB) mRNA expression. Data represent the means +/− standard errors of the means from three independent experiments. *p < 0.05; ***p < 0.001 (by an unpaired two-tailed *t*-test).

(F) Levels of ATGL, HSL, and MGL mRNA expression were detected by RT-qPCR. RNA was extracted from stably expressing sh-SMPDL3B or sh-control cells. Values were normalized to the level of β-actin (ACTB) mRNA expression. Data represent the means +/− standard errors of the means from three independent experiments. *p < 0.05; **p < 0.01; (by an unpaired two-tailed *t*-test).

(G) Immunoblot analysis of protein expression in cells from panel 7E and F. Antibodies used in the experiments are indicated on the left (FASN: Rabbit anti-FASN antibody; ACC: Rabbit anti-ACC antibody; ATGL: Rabbit anti-ATGL antibody; β-actin: Sheep anti-rabbit antibody).

(H) SMPDL3B-rescue cells were stained with oil red O. Cells were fixed with 4% paraformaldehyde, stained with oil red O, and counterstained with hematoxylin. The bottom image corresponds to the boxed region marked in the upper image. Each image is representative of three independent experiments.

(I) Number of LDS per cell. The number of LDS per cell was quantified in each image. At least 80 cells were counted. Data are representative of the means +/− standard errors of the means from three independent experiments. **p < 0.01; ns, not significant (by an unpaired two-tailed *t*-test).

sialoadhesin,[46] vimentin,[47] cluster of differentiation 151,[48] non-muscle myosin heavy chain IIA,[49] and DC-SIGN (CD209).[50] A defect in any of these functional factors will affect the replication of PRRSV; however, the threat of PRRSV to pigs has become increasingly more serious, indicating an urgent need for additional PRRSV research. In this study, we showed that a SMPDL3B deficiency had a strong inhibitory effect on PRRSV replication by regulating lipid metabolism.

We have shown that SMPDL3B is ubiquitously expressed in many species (Figure 2A). SMPDL3B is also prevalent in various pig tissues, with the highest expression in white adipose tissue and lung (Figure 2B). This finding suggests that SMPDL3B is related to lipid droplet storage (LDS) and the reason the lung was used as a target organ. In this study, we have demonstrated that PRRSV (HP-PRRSV/LP-PRRSV) infection gradually increased the level of SMPDL3B mRNA and protein expression in MARC-145 and PAMs cells (Figure 3). In addition, a SMPDL3B deficiency reduced the level of PRRSV mRNA and protein expression (Figure 4), and SMPDL3B-rescue cells remove the inhibition of PRRSV replication due to SMPDL3B deficiency (Figures 3L–3O), suggesting that SMPDL3B knockout inhibits PRRSV replication and that SMPDL3B plays a positive role in PRRSV replication. As is shown in Figure 5, SMPDL3B overexpression promoted PRRSV replication (Figure 5), suggesting that SMPDL3B functions as a host factor to promote PRRSV replication again. Currently, the mechanism by which SMPDL3B affects PRRSV proliferation remains unclear. Viruses hijack hosts to perform numerous tasks during their replication cycles, and the role of virus associated with LDS in the life cycle has not been well established.

Early research indicates that LDs are associated with Hepatitis C virus assembly[51,52] and the assembly of the rotavirus outer capsid, which is related to LDs.[53] In a recent study, it showed that PRRSV is related to lipophagy.[28] In this study, we show that a SMPDL3B deficiency reduces the attachment, entry, replication, and secretion of PRRSV, but not assembly (Figure 6). These results are consistent with previous findings, suggesting that LDs are important for viral replication. LDs participate in most cellular processes, including energy storage and second messengers in signaling events.[54,55] In addition, most cellular processes associated with LDs are closely related to lipid rafts. Indeed, it has previously been reported that SMPDL3B plays an important role in lipid rafts.[56] SMPDL3B has been implicated in many cellular functions, and recent evidence suggests that SMPDL3B is involved in TLR signaling.[26,57] Moreover, SMPDL3B mediates radiation-induced damage to renal podocytes[58] and is also involved in diabetic kidney disease.[56,59] Although studies have highlighted the significance of SMPDL3B in maintaining normal lipid metabolism, the mechanism by which SMPDL3B functions as a host factor during PRRSV infection remains unclear. Therefore, we assessed the impact of a SMPDL3B

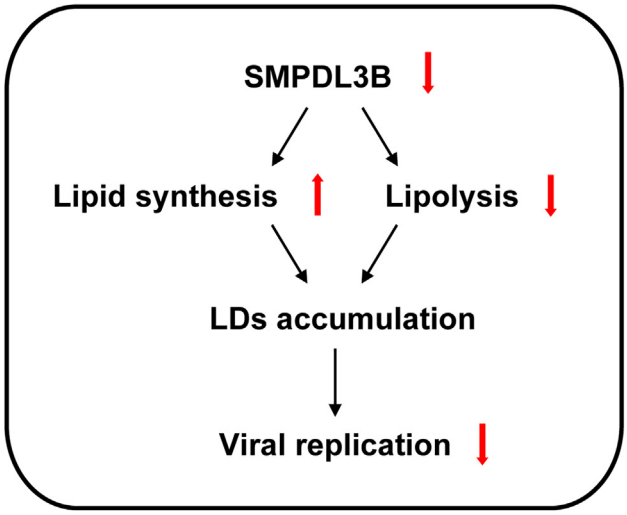

Figure 8. The knockdown of SMPDL3B promotes the expression of lipid synthesis genes and inhibits the expression of lipid breakdown genes, leading to the accumulation of lipid droplets (LDS)
Due to the knockdown of SMPDL3B, the utilization of lipids is inhibited, resulting in the inhibition of PRRSV replication.

knockdown on LDs. Figure 6 shows that the expression of key lipid synthesis genes (FASN, ACC1, and SCD-1) was significantly increased, whereas the expression of lipid lipolysis genes (ATGL, HSL, and HSL) was reduced. We confirmed that SMPDL3B function is mediated jointly by the expression of these key genes (Figure 6). Furthermore, the level of ATGL mRNA expression was significantly reduced (Figure 6). There results suggested that SMPDL3B affects PRRSV replication by regulating lipid metabolism. As shown in Figure 7, the number of LDs in SMPDL3B complemented cells was significantly lower than that in SMPDL3B-deficient cells, indicating that SMPDL3B negatively regulates LD formation, consistent with previous experiments and verification tests.[26,27] These results confirm that PRRSV upregulates SMPDL3B to promote viral replication through modulation of lipid metabolism (Figure 8).

In this study, we have shown that SMPDL3B positively regulates PRRSV replication. Additionally, PRRSV replication can be blunted in SMPDL3B-deficient cells. This may be due to the defect of SMPDL3B, which leads to an inhibition of ATGL activity and greatly inhibits PRRSV replication. Thus, we have identified SMPDL3B as a novel host factor important for the replication of PRRSV. We have also identified a new function for SMPDL3B in regulating lipid metabolism. Further studies on the mechanism by which SMPDL3B deficiency inhibits viral replication (PRV/VSV) are ongoing.

Limitations of the study

Although we employed multiple mature techniques and provided multiple perspectives to demonstrate the regulation of PRRSV replication by SMPDL3B via lipids, some limitations still exist. (1) There have been no reports on SMPDL3B gene-edited pigs, which prevented us from verifying the replication of PRRSV in SMPDL3B gene-edited pigs. (2) The use of transfection reagents in constructing the knocked-down cell line using CRISPR-Cas9 technology may lead to some toxicity to the cells, which could result in experimental deviations. Nevertheless, our experiments confirmed that SMPDL3B regulates PRRSV replication via lipids, and we hope that our current research can promote the application of CRISPR-Cas9 technology in virus research and animal health.

STAR★METHODS

Detailed methods are provided in the online version of this paper and include the following:

- KEY RESOURCES TABLE
- RESOURCE AVAILABILITY
  - Lead contact
  - Materials availability

ACKNOWLEDGMENTS

This research is supported by grants from Chengdu Key R&D Support Plan Project (2022-YF09-00050-SN) and the Doctoral Foundation of Henan Agricultural University (30501221).

AUTHOR CONTRIBUTIONS

Conceptualization: H.-H.S., Q.Z., Y.-P.W., R.W., S.-Y.D., X.-B.H., X.T.W., S.-J.C., L.Z., Q.-G.Y. Methodology: H.-H.S. Writing - Original Draft Preparation: L.Z., Q.-G.Y. Writing - Review & Editing: L.Z., Q.-G.Y. Supervision: L.Z., Q.-G.Y. Funding Acquisition: L.Z., Q.-G.Y.

DECLARATION OF INTERESTS

The authors declare no conflicts of interest.

INCLUSION AND DIVERSITY

We worked to ensure that the study questionnaires were prepared in an inclusive way.

We worked to ensure diversity in experimental samples through the selection of the cell lines.

We worked to ensure diversity in experimental samples through the selection of the genomic datasets.

We avoided "helicopter science" practices by including the participating local contributors from the region where we conducted the research as authors on the paper.

Received: April 20, 2023
Revised: June 4, 2023
Accepted: July 17, 2023
Published: July 22, 2023

REFERENCES

1. Lunney, J.K., Fang, Y., Ladinig, A., Chen, N., Li, Y., Rowland, B., and Renukaradhya, G.J. (2016). Porcine Reproductive and Respiratory Syndrome Virus (PRRSV): Pathogenesis and Interaction with the Immune System. Annu. Rev. Anim. Biosci. *4*, 129–154. https://doi.org/10.1146/annurev-animal-022114-111025.

2. Olanratmanee, E.O., Thanawongnuwech, R., Kunavongkrit, A., and Tummaruk, P. (2014). Reproductive performance of sows with and without PRRS modified live virus vaccination in PRRS-virus-seropositive herds. Trop. Anim. Health Prod. *46*, 1001–1007. https://doi.org/10.1007/s11250-014-0606-5.

3. Bilodeau, R., Dea, S., Sauvageau, R.A., and Martineau, G.P. (1991). 'Porcine reproductive and respiratory syndrome' in Quebec. Vet. Rec. *129*, 102–103. https://doi.org/10.1136/vr.129.5.102.

4. Christianson, W.T., Collins, J.E., Benfield, D.A., Harris, L., Gorcyca, D.E., Chladek, D.W., Morrison, R.B., and Joo, H.S. (1992). Experimental reproduction of swine infertility and respiratory syndrome in pregnant sows. Am. J. Vet. Res. *53*, 485–488.

5. Halbur, P.G., Paul, P.S., Frey, M.L., Landgraf, J., Eernisse, K., Meng, X.J., Lum, M.A., Andrews, J.J., and Rathje, J.A. (1995). Comparison of the pathogenicity of two US porcine reproductive and respiratory syndrome virus isolates with that of the Lelystad virus. Vet. Pathol. *32*, 648–660. https://doi.org/10.1177/030098589503200606.

6. Pol, J.M., van Dijk, J.E., Wensvoort, G., and Terpstra, C. (1991). Pathological, ultrastructural, and immunohistochemical changes caused by Lelystad virus in experimentally induced infections of mystery

swine disease (synonym: porcine epidemic abortion and respiratory syndrome (PEARS)). Vet. Q. *13*, 137–143. https://doi.org/10.1080/01652176.1991.9694298.

7. Snijder, E.J., Kikkert, M., and Fang, Y. (2013). Arterivirus molecular biology and pathogenesis. J. Gen. Virol. *94*, 2141–2163. https://doi.org/10.1099/vir.0.056341-0.

8. García-Sastre, A. (2010). Influenza virus receptor specificity: disease and transmission. Am. J. Pathol. *176*, 1584–1585. https://doi.org/10.2353/ajpath.2010.100066.

9. Jusa, E.R., Inaba, Y., Kouno, M., and Hirose, O. (1997). Effect of heparin on infection of cells by porcine reproductive and respiratory syndrome virus. Am. J. Vet. Res. *58*, 488–491.

10. Delputte, P.L., Costers, S., and Nauwynck, H.J. (2005). Analysis of porcine reproductive and respiratory syndrome virus attachment and internalization: distinctive roles for heparan sulphate and sialoadhesin. J. Gen. Virol. *86*, 1441–1445. https://doi.org/10.1099/vir.0.80675-0.

11. Keiser, N., Venkataraman, G., Shriver, Z., and Sasisekharan, R. (2001). Direct isolation and sequencing of specific protein-binding glycosaminoglycans. Nat. Med. *7*, 123–128. https://doi.org/10.1038/83263.

12. Burkard, C., Lillico, S.G., Reid, E., Jackson, B., Mileham, A.J., Ait-Ali, T., Whitelaw, C.B.A., and Archibald, A.L. (2017). Precision engineering for PRRSV resistance in pigs: Macrophages from genome edited pigs lacking CD163 SRCR5 domain are fully resistant to both PRRSV genotypes while maintaining biological function. PLoS Pathog. *13*, e1006206. https://doi.org/10.1371/journal.ppat.1006206.

13. Burkard, C., Opriessnig, T., Mileham, A.J., Stadejek, T., Ait-Ali, T., Lillico, S.G., Whitelaw, C.B.A., and Archibald, A.L. (2018). Pigs Lacking the Scavenger Receptor Cysteine-Rich Domain 5 of CD163 Are Resistant to Porcine Reproductive and Respiratory Syndrome Virus 1 Infection. J. Virol. *92*, e00415-18. https://doi.org/10.1128/jvi.00415-18.

14. Yang, H., Zhang, J., Zhang, X., Shi, J., Pan, Y., Zhou, R., Li, G., Li, Z., Cai, G., and Wu, Z. (2018). CD163 knockout pigs are fully resistant to highly pathogenic porcine reproductive and respiratory syndrome virus. Antivir. Res. *151*, 63–70. https://doi.org/10.1016/j.antiviral.2018.01.004.

15. Lager, K.M., Schlink, S.N., Brockmeier, S.L., Miller, L.C., Henningson, J.N., Kappes, M.A., Kehrli, M.E., Loving, C.L., Guo, B., Swenson, S.L., et al. (2014). Efficacy of Type 2 PRRSV vaccine against Chinese and Vietnamese HP-PRRSV challenge in pigs. Vaccine *32*, 6457–6462. https://doi.org/10.1016/j.vaccine.2014.09.046.

16. Goñi, F.M., and Alonso, A. (2002). Sphingomyelinases: enzymology and membrane activity. FEBS Lett. *531*, 38–46. https://doi.org/10.1016/s0014-5793(02)03482-8.

17. Marchesini, N., and Hannun, Y.A. (2004). Acid and neutral sphingomyelinases: roles and mechanisms of regulation. Biochem. Cell Biol. *82*, 27–44. https://doi.org/10.1139/o03-091.

18. Hannun, Y.A., and Obeid, L.M. (2011). Many ceramides. J. Biol. Chem. *286*, 27855–27862. https://doi.org/10.1074/jbc.R111.254359.

19. Seto, M., Whitlow, M., McCarrick, M.A., Srinivasan, S., Zhu, Y., Pagila, R., Mintzer, R., Light, D., Johns, A., and Meurer-Ogden, J.A. (2004). A model of the acid sphingomyelinase phosphoesterase domain based on its remote structural homolog purple acid phosphatase. Protein Sci. *13*, 3172–3186. https://doi.org/10.1110/ps.04966204.

20. Pattingre, S., Bauvy, C., Levade, T., Levine, B., and Codogno, P. (2009). Ceramide-induced autophagy: to junk or to protect cells? Autophagy *5*, 558–560. https://doi.org/10.4161/auto.5.4.8390.

21. Stiban, J., Tidhar, R., and Futerman, A.H. (2010). Ceramide synthases: roles in cell physiology and signaling. Adv. Exp. Med. Biol. *688*, 60–71. https://doi.org/10.1007/978-1-4419-6741-1_4.

22. Goldkorn, T., and Filosto, S. (2010). Lung injury and cancer: Mechanistic insights into ceramide and EGFR signaling under cigarette smoke. Am. J. Respir. Cell Mol. Biol. *43*, 259–268. https://doi.org/10.1165/rcmb.2010-0220RT.

23. Liu, B., Xiao, J., Dong, M., Qiu, Z., and Jin, J. (2020). Human alkaline ceramidase 2 promotes the growth, invasion, and migration of hepatocellular carcinoma cells via sphingomyelin phosphodiesterase acid-like 3B. Cancer Sci. *111*, 2259–2274. https://doi.org/10.1111/cas.14453.

24. Masuishi, Y., Nomura, A., Okayama, A., Kimura, Y., Arakawa, N., and Hirano, H. (2013). Mass spectrometric identification of glycosylphosphatidylinositol-anchored peptides. J. Proteome Res. *12*, 4617–4626. https://doi.org/10.1021/pr4004807.

25. Abou Daher, A., Francis, M., Azzam, P., Ahmad, A., Eid, A.A., Fornoni, A., Marples, B., and Zeidan, Y.H. (2020). Modulation of radiation-induced damage of human glomerular endothelial cells by SMPDL3B. FASEB. J. *34*, 7915–7926. https://doi.org/10.1096/fj.201902179R.

26. Heinz, L., Baumann, C., K?Berlin, M., Snijder, B., Gawish, R., Shui, G., Sharif, O., Aspalter, I., Müller, A., and Kandasamy, R.J.C.R. (2015). The Lipid-Modifying Enzyme SMPDL3B Negatively Regulates Innate Immunity, *11*.

27. Mallela, S.K., Ge, M., Molina, J., Santos, J.V., Kim, J.J., Mitrofanova, A., Al-Ali, H., Marples, B., Merscher, S., and Fornoni, A. (2022). Sphingomyelin phosphodiesterase acid like 3B (SMPDL3b) regulates Perilipin5 (PLIN5) expression and mediates lipid droplet formation. Genes Dis. *9*, 1397–1400. https://doi.org/10.1016/j.gendis.2021.12.014.

28. Wang, J., Liu, J.Y., Shao, K.Y., Han, Y.Q., Li, G.L., Ming, S.L., Su, B.Q., Du, Y.K., Liu, Z.H., Zhang, G.P., et al. (2019). Porcine Reproductive and Respiratory Syndrome Virus Activates Lipophagy To Facilitate Viral Replication through Downregulation of NDRG1 Expression. J. Virol. *93*, e00526-19. https://doi.org/10.1128/jvi.00526-19.

29. Currie, E., Schulze, A., Zechner, R., Walther, T.C., and Farese, R.V., Jr. (2013). Cellular fatty acid metabolism and cancer. Cell Metabol. *18*, 153–161. https://doi.org/10.1016/j.cmet.2013.05.017.

30. Ducharme, N.A., and Bickel, P.E. (2008). Lipid droplets in lipogenesis and lipolysis. Endocrinology *149*, 942–949. https://doi.org/10.1210/en.2007-1713.

31. Stapleford, K.A., and Miller, D.J. (2010). Role of cellular lipids in positive-sense RNA virus replication complex assembly and function. Viruses *2*, 1055–1068. https://doi.org/10.3390/v2051055.

32. Lorizate, M., and Kräusslich, H.G. (2011). Role of lipids in virus replication. Cold Spring Harbor Perspect. Biol. *3*, a004820. https://doi.org/10.1101/cshperspect.a004820.

33. Huang, L., Zhang, Y.P., Yu, Y.L., Sun, M.X., Li, C., Chen, P.Y., and Mao, X. (2011). Role of lipid rafts in porcine reproductive and respiratory syndrome virus infection in MARC-145 cells. Biochem. Biophys. Res. Commun. *414*, 545–550. https://doi.org/10.1016/j.bbrc.2011.09.109.

34. Ke, W., Fang, L., Jing, H., Tao, R., Wang, T., Li, Y., Long, S., Wang, D., and Xiao, S. (2017). Cholesterol 25-Hydroxylase Inhibits Porcine Reproductive and Respiratory Syndrome Virus Replication through Enzyme Activity-Dependent and -Independent Mechanisms. J. Virol. *91*, e00827-17. https://doi.org/10.1128/jvi.00827-17.

35. Kristensen, C.S., Kvisgaard, L.K., Pawlowski, M., Holmgaard Carlsen, S., Hjulsager, C.K., Heegaard, P.M.H., Bøtner, A., Stadejek, T., Haugegaard, S., and Larsen, L.E. (2018). Efficacy and safety of simultaneous vaccination with two modified live virus vaccines against porcine reproductive and respiratory syndrome virus types 1 and 2 in pigs. Vaccine *36*, 227–236. https://doi.org/10.1016/j.vaccine.2017.11.059.

36. Heinz, L.X., Baumann, C.L., Köberlin, M.S., Snijder, B., Gawish, R., Shui, G., Sharif, O., Aspalter, I.M., Müller, A.C., Kandasamy, R.K., et al. (2015). The Lipid-Modifying Enzyme SMPDL3B Negatively Regulates Innate Immunity. Cell Rep. *11*, 1919–1928. https://doi.org/10.1016/j.celrep.2015.05.006.

37. Zhu, Z., Zhang, X., Dong, W., Wang, X., He, S., Zhang, H., Wang, X., Wei, R., Chen, Y., Liu, X., and Guo, C. (2020). TREM2 suppresses the proinflammatory response to facilitate PRRSV infection via PI3K/NF-κB signaling. PLoS Pathog. *16*, e1008543. https://doi.org/10.1371/journal.ppat.1008543.

38. Qiu, B., and Simon, M.C. (2016). BODIPY 493/503 Staining of Neutral Lipid Droplets for Microscopy and Quantification by Flow Cytometry. Bio. Protoc. *6*, e1912. https://doi.org/10.21769/BioProtoc.1912.

39. Mao, Y., Zhang, Z., Feng, Z., Wei, P., Zhang, H., Botella, J.R., and Zhu, J.K. (2016). Development of germ-line-specific CRISPR-Cas9 systems to improve the production of heritable gene modifications in Arabidopsis. Plant Biotechnol. J. *14*, 519–532. https://doi.org/10.1111/pbi.12468.

40. Kim, H., Kim, S.T., Ryu, J., Choi, M.K., Kweon, J., Kang, B.C., Ahn, H.M., Bae, S., Kim, J., Kim, J.S., and Kim, S.G. (2016). A simple, flexible and high-throughput cloning system for plant genome editing via CRISPR-Cas system. J. Integr. Plant Biol. *58*, 705–712. https://doi.org/10.1111/jipb.12474.

41. Bae, S.J., Park, B.G., Kim, B.G., and Hahn, J.S. (2020). Multiplex Gene Disruption by Targeted Base Editing of Yarrowia lipolytica Genome Using Cytidine Deaminase Combined with the CRISPR/Cas9 System. Biotechnol. J. *15*, e1900238. https://doi.org/10.1002/biot.201900238.

42. Johnson, R.A., Gurevich, V., Filler, S., Samach, A., and Levy, A.A. (2015). Comparative assessments of CRISPR-Cas nucleases' cleavage efficiency *in planta*. Plant Mol. Biol. *87*, 143–156. https://doi.org/10.1007/s11103-014-0266-x.

43. Xu, R., Li, H., Qin, R., Wang, L., Li, L., Wei, P., and Yang, J. (2014). Gene targeting using the Agrobacterium tumefaciens-mediated CRISPR-Cas system in rice. Rice *7*, 5. https://doi.org/10.1186/s12284-014-0005-6.

44. Guo, L., Niu, J., Yu, H., Gu, W., Li, R., Luo, X., Huang, M., Tian, Z., Feng, L., and Wang, Y. (2014). Modulation of CD163 expression by metalloprotease ADAM17 regulates porcine reproductive and respiratory syndrome virus entry. J. Virol. *88*, 10448–10458. https://doi.org/10.1128/jvi.01117-14.

45. Delputte, P.L., Vanderheijden, N., Nauwynck, H.J., and Pensaert, M.B. (2002). Involvement of the matrix protein in attachment of porcine reproductive and respiratory syndrome virus to a heparinlike receptor on porcine alveolar macrophages. J. Virol. *76*, 4312–4320. https://doi.org/10.1128/jvi.76.9.4312-4320.2002.

46. Delputte, P.L., Van Breedam, W., Delrue, I., Oetke, C., Crocker, P.R., and Nauwynck, H.J. (2007). Porcine arterivirus attachment to the macrophage-specific receptor sialoadhesin is dependent on the sialic acid-binding activity of the N-terminal immunoglobulin domain of sialoadhesin. J. Virol. *81*, 9546–9550. https://doi.org/10.1128/jvi.00569-07.

47. Kim, J.K., Fahad, A.M., Shanmukhappa, K., and Kapil, S. (2006). Defining the cellular target(s) of porcine reproductive and respiratory syndrome virus blocking monoclonal antibody 7G10. J. Virol. *80*, 689–696. https://doi.org/10.1128/jvi.80.2.689-696.2006.

48. Wu, J., Peng, X., Zhou, A., Qiao, M., Wu, H., Xiao, H., Liu, G., Zheng, X., Zhang, S., and Mei, S. (2014). MiR-506 inhibits PRRSV replication in MARC-145 cells via CD151. Mol. Cell. Biochem. *394*, 275–281. https://doi.org/10.1007/s11010-014-2103-6.

49. Gao, J., Xiao, S., Xiao, Y., Wang, X., Zhang, C., Zhao, Q., Nan, Y., Huang, B., Liu, H., Liu, N., et al. (2016). MYH9 is an Essential Factor for Porcine Reproductive and Respiratory Syndrome Virus Infection. Sci. Rep. *6*, 25120. https://doi.org/10.1038/srep25120.

50. Piñeyro, P.E., Subramaniam, S., Kenney, S.P., Heffron, C.L., Giménez-Lirola, L.G., and Meng, X.J. (2016). Modulation of Proinflammatory Cytokines in Monocyte-Derived Dendritic Cells by Porcine Reproductive and Respiratory Syndrome Virus Through Interaction with the Porcine Intercellular-Adhesion-Molecule-3-Grabbing Nonintegrin. Viral Immunol. *29*, 546–556. https://doi.org/10.1089/vim.2016.0104.

51. McLauchlan, J., Lemberg, M.K., Hope, G., and Martoglio, B. (2002). Intramembrane proteolysis promotes trafficking of hepatitis C virus core protein to lipid droplets. EMBO J. *21*, 3980–3988. https://doi.org/10.1093/emboj/cdf414.

52. Hourioux, C., Ait-Goughoulte, M., Patient, R., Fouquenet, D., Arcanger-Doudet, F., Brand, D., Martin, A., and Roingeard, P. (2007). Core protein domains involved in hepatitis C virus-like particle assembly and budding at the endoplasmic reticulum membrane. Cell Microbiol. *9*, 1014–1027. https://doi.org/10.1111/j.1462-5822.2006.00848.x.

53. Trask, S.D., McDonald, S.M., and Patton, J.T. (2012). Structural insights into the coupling of virion assembly and rotavirus replication. Nat. Rev. Microbiol. *10*, 165–177. https://doi.org/10.1038/nrmicro2673.

54. Hannun, Y.A., and Obeid, L.M. (2008). Principles of bioactive lipid signalling: lessons from sphingolipids. Nat. Rev. Mol. Cell Biol. *9*, 139–150. https://doi.org/10.1038/nrm2329.

55. van Meer, G., Voelker, D.R., and Feigenson, G.W. (2008). Membrane lipids: where they are and how they behave. Nat. Rev. Mol. Cell Biol. *9*, 112–124. https://doi.org/10.1038/nrm2330.

56. Mitrofanova, A., Mallela, S.K., Ducasa, G.M., Yoo, T.H., Rosenfeld-Gur, E., Zelnik, I.D., Molina, J., Varona Santos, J., Ge, M., Sloan, A., et al. (2019). SMPDL3b modulates insulin receptor signaling in diabetic kidney disease. Nat. Commun. *10*, 2692. https://doi.org/10.1038/s41467-019-10584-4.

57. Watanabe, S., Hidenori, U., Hashimoto, S., Riko, S., Aizawa, T., Tsugawa, K., Imaizumi, T., and Tanaka, H. (2022). Sphingomyelin Phosphodiesterase Acid-Like 3b is Essential for Toll-Like Receptor 3 Signaling in Human Podocytes. J. Membr. Biol. *255*, 117–122. https://doi.org/10.1007/s00232-021-00206-w.

58. Ahmad, A., Mitrofanova, A., Bielawski, J., Yang, Y., Marples, B., Fornoni, A., and Zeidan, Y.H. (2017). Sphingomyelinase-like phosphodiesterase 3b mediates radiation-induced damage of renal podocytes. FASEB. J. *31*, 771–780. https://doi.org/10.1096/fj.201600618R.

59. Yoo, T.H., Pedigo, C.E., Guzman, J., Correa-Medina, M., Wei, C., Villarreal, R., Mitrofanova, A., Leclercq, F., Faul, C., Li, J., et al. (2015). Sphingomyelinase-like phosphodiesterase 3b expression levels determine podocyte injury phenotypes in glomerular disease. J. Am. Soc. Nephrol. *26*, 133–147. https://doi.org/10.1681/asn.2013111213.

STAR★METHODS

KEY RESOURCES TABLE

REAGENT or RESOURCE	SOURCE	IDENTIFIER
Antibodies		
anti-PRRSV nucleocapsid (N) antibody SDOW17	Rural Technologies	N/A
anti-FASN antibody	CST	Cat# 3180; RRID:AB_2100796
anti-ACC	CST	Cat# 3662; RRID:AB_2219400
anti-ATGL	CST	Cat# 2138; RRID:AB_2167955
mouse monoclonal anti-dsRNA antibody	CST	Cat# 76651; RRID:AB_2936194
anti-mouse IgG antibody labeled with Alexa Fluor 555	Thermo Fisher Scientific	Cat# A-21424; RRID:AB_141780
anti-SMPDL3B antibody	Proteintech	Cat# 16552-1-AP; RRID:AB_2878276
anti-rabbit IgG antibody labeled with Alexa Fluor 488	Thermo Fisher Scientific	Cat# A-11034;RRID:AB_2576217
Bacterial and virus strains		
PRRSV-VR2332	Jiang wang gave a gift	N/A
PRRSV-JXA1	Jiang wang gave a gift	N/A
PRRSV-GFP	En-Min Zhou gave a gift	N/A
VSV-GFP	Jiang wang gave a gift	N/A
PRV-GFP	Jiang wang gave a gift	N/A
Chemicals, peptides, and recombinant proteins		
TRIzol reagent	TaKaRa Bio Inc	D9108B
SYBR premix Ex Taq	TaKaRa Bio Inc	RR420A
PrimeScript™ RT reagent Kit with gDNA Eraser (Perfect Real Time)	TaKaRa Bio Inc	RR047A
SuperKine™ Maximum Sensitivity Cell Counting Kit-8 (CCK-8)	Abbkine Scientific (Wuhan, China);	BMU106-CN
oil red O	Sigma-Aldrich	1320-06-5
BODIPY 493/503	Thermo Fisher Scientific	121207-31-6
assay kit for free fatty acids	APPLYGEN	E1001
Tissue Cell Total Cholesterol (TC) Content Enzymatic Determination Kit	APPLYGEN	E1015-105
Tissue Cell Triglyceride (TG) Content Enzymatic Determination Kit	APPLYGEN	E1013-50
RIPA Lysis Buffer (strong)	Beyotime Biotechnology	P0013B
Lipofectamine 3000	Invitrogen	L3000015
Deposited data		
This study did not generate new unique reagents		
Porcine reproductive and respiratory syndrome virus upregulates SMPDL3B to promote viral replication by modulating lipid metabolism	https://data.mendeley.com/	Database: https://doi.org/10.17632/3ctpx4k6jp.2
Experimental models: Cell lines		
3D4/21-CD163	En-Min Zhou gave a gift	RRID : CVCL_VG78

(*Continued on next page*)

Continued

REAGENT or RESOURCE	SOURCE	IDENTIFIER
MARC-145	ATCC	HTX1894; RRID : CVCL_4540
PAM	Jiang wang gave a gift	N/A
293T/17	ATCC	CRL-11268; RRID:CVCL_UE07
Experimental model and study participants		
Qi-Gui Yan[1,#]	52-year-old	male
Lei Zeng[2,#]	34-year-old	male
Huan-Huan Shen	34-year-old	male
No animal models		
Oligonucleotides		
ShRNA-1 targeting SMPDL3B sequence: Top Strand: **CCGG**GGACTACAAGGTATCTCAAGACTC GAGTCTTGAGATACCTTGTAGTCC**TTTTTG** Bottom Strand: **AATTCAAAAA**GGACTACAA GGTATCTCAAGACTCGAGTCTTGAGATACC TTGTAGTCC	This paper	N/A
ShRNA-2 targeting SMPDL3B sequence: Top Strand: **CCGG**GCTCATCAGAGAGG TCTTTCCCTCGAGGGAAAGACCTCTCT GATGAGC**TTTTTG** Bottom Strand: **AATTCAAAAA**GCTCATCAG AGAGGTCTTTCCCTCGAGGGAAAGACCTC TCTGATGAGC	This paper	N/A
ShRNA-1 targeting GPS2-1 sequence: Top Strand: **CCGG**GCCTCGACTCCGGAAGG ATTCCTCGAGGAATCCTTC CGGAGTCGAGGC**TTTTTG** Bottom Strand: **AATTCAAAAA**GCCTCGACTC CGGAAGGATTCCTCGAGGAATCCTTCCGGA GTCGAGGC	This paper	N/A
ShRNA-1 targeting GPS2-2 sequence: Top Strand: **CCGG**GACAGCCTCGACTCCGGAAGGCTCG AGCCTTCCGGAGTCGAGGCTGTC**TTTTTG** Bottom Strand: **AATTCAAAAA**GACAGCCTCG ACTCCGGAAGGCTCGAGCCTTCCGGAGTCG AGGCTGTC	This paper	N/A
ShRNA-1 targeting FGF10-1 sequence: Top Strand: **CCGG**GCTGAAACTCTAGTCCCTTAGCT CGAGCTAAGGGACTAGAGTTTCAGC **TTTTTG** Bottom Strand: **AATTCAAAAA**GCTGAAA CTCTAGTCCCTTAGCTCGAGCTAAGGG ACTAGAGTTTCAGC	This paper	N/A

(*Continued on next page*)

Continued

REAGENT or RESOURCE	SOURCE	IDENTIFIER
ShRNA-1 targeting FGF10-2 sequence: Top Strand: **CCGG**GCATTTGTCAGCTCACATATACTCGA GTATATGTGAGCTGACAAATGC**TTTTTG** Bottom Strand: **AATTCAAAAA**GCATTTGTCA GCTCACATATACTCGAGTATATGTGAGCTG ACAAATGC	This paper	N/A
ShRNA-1 targeting KCNC2-1 sequence: Top Strand: **CCGG**GCGGGAATAGAAA GGATATGGCTCGAGCCATATCCTTTCT ATTCCCGC**TTTTTG** Bottom Strand: **AATTCAAAAA**GCGGGA ATAGAAAGGATATGGCTCGAGCCATAT CCTTTCTATTCCCGC	This paper	N/A
ShRNA-1 targeting KCNC2-2 sequence: Top Strand: **CCGG**GGTGATTACACGTG TGCTTCTCTCGAGAGAAGCACACGTGT AATCACC**TTTTTG** Bottom Strand: **AATTCAAAAA**GGTGATT ACACGTGTGCTTCTCTCGAGAGAAGCA CACGTGTAATCACC	This paper	N/A
ShRNA-1 targeting MGAT5B-1 sequence: Top Strand: **CCGG**GCTTCTTCTCACTCT GCTTCCCGAAGGAAGCAGAGTGAGAA GAAGC**TTTTTG** Bottom Strand: **AATTCAAAAA**GCTTCTT CTCACTCTGCTTCCTTCGGGAAGCAGA GTGAGAAGAAGC	This paper	N/A
ShRNA-1 targeting MGAT5B-2 sequence: Top Strand: **CCGG**GGAAGGAGTCTCTAA TCTTTACGAATAAAGATTAGAGACTCCTT CC**TTTTTG** Bottom Strand: **AATTCAAAAA**GGAAGGA GTCTCTAATCTTTATTCGTAAAGATTAGA GACTCCTTCC	This paper	N/A
sgRNA targeting SMPDL3B sequence: Top Strand: AAACTCCACTGAGCTCTTTTGC Bottom Strand: CTTGGTCTTTTCAAGCCTCTGT	This paper	N/A
p3xFLAG-CMV-14 targeting SMPDL3B sequence: Top Strand: CAGGGATGCCACCCGGGATCCTCA GCTTTGGATAAATGG Bottom Strand: AAGGATGACGATGACAAGCTTATG AAAAGTCAGAGGAGC	This paper	N/A
Primers used for SMPDL3B RT-qPCR analysis Top Strand: CAGCATAGACTTGAGTATCTGGAAA Bottom Strand: GGGGACTACCTCTGCGATTC	This paper	N/A
Primers used for FGF10 RT-qPCR analysis Top Strand: TGTTGCTGTTCTTGGTGTCTTC Bottom Strand: AGAGAATAGCTTTCTCCAGCGG	This paper	N/A
Primers used for GPS2 RT-qPCR analysis Top Strand: GGAACAAATCCTGAAGTTGCAGG Bottom Strand: ATGCTGAGGAGGTGAGTTCCT	This paper	N/A

(*Continued on next page*)

Continued

REAGENT or RESOURCE	SOURCE	IDENTIFIER
Primers used for MGAT5B RT-qPCR analysis Top Strand: TGCTTCTGCACAGCAAGGTG Bottom Strand: CAAAACCACTCGACCTCACTG	This paper	N/A
Primers used for KCNC2 RT-qPCR analysis Top Strand: TTCTTCTTCGACCGGCACCC Bottom Strand: TCTCGAAGATGTCGAGCGCC	This paper	N/A
Primers used for GADPH RT-qPCR analysis Top Strand: AAGTTCCACGGCACAGTCAA Bottom Strand: GCCTTCTCCATGGTCGTGAA	This paper	N/A
Primers used for β-actin RT-qPCR analysis Top Strand: CTGAACCCCAAAGCCAACCGT Bottom Strand: TTCTCCTTGATGTCCCGCACG	This paper	N/A
Primers used for Chlorocebus-β-actin RT-qPCR analysis Top Strand: CGTGGACATCCGTAAAGAC Bottom Strand: GGAAGGTGGACAGCGAGGC	This paper	N/A
Primers used for PRRSV ORF7 RT-qPCR analysis Top Strand: AAACCAGTCCAGAGGCAAGG Bottom Strand: GCAAACTAAACTCCACAGTGTAA	This paper	N/A
Primers used for ACC1 RT-qPCR analysis Top Strand: GGAGACAAACAGGGACCATTACA Bottom Strand: CAGGGACTGCCGAAACATC	This paper	N/A
Primers used for FASN RT-qPCR analysis Top Strand: TGCTCCTGCACGTCTCCC Bottom Strand: CTGCTGAAGCCTAACTCCTCG	This paper	N/A
Primers used for SCD RT-qPCR analysis Top Strand: AATGGAGGGGGCAAGTTGGA Bottom Strand: GGTGGGGATCAATATGATCCC	This paper	N/A
Primers used for ATGL analysis Top Strand: TGTGGCCTCATTCCTCCTAC Bottom Strand: TCGTGGATGTTGGTGGAGCT	This paper	N/A
Primers used for HSL analysis Top Strand: TCAGGTGTCTTTGCGGGTAT Bottom Strand: CTTGTGCGGAAGAAGATGCT	This paper	N/A
Primers used for TNF-α analysis Top Strand: CTGTAGGTTGCTCCCACCTG Bottom Strand: CCAGTAGGGCGGTTACAGAC	This paper	N/A
Primers used for IL-6 analysis Top Strand: TGATGCCACCTCAGACAA Bottom Strand: CACACTTCTCATACTTCTCAC	This paper	N/A
Primers used for IL-8 analysis Top Strand: CAGTTCTGGCAAGAGTAAGT Bottom Strand: CTCAATCACTCTCAGTTCCTT	This paper	N/A
Primers used for IL-1β analysis Top Strand: TGGAACAAGAGCATCAGGCA Bottom Strand: AGACTGCACGTTGGCATCAC	This paper	N/A
Recombinant DNA		
p3xFLAG-CMV-14	addgene	#59974; RRID:Addgene_59974
pLKO.1 puro	addgene	#8453; RRID:Addgene_8453
lentiCRISPR v2-puro	addgene	#52961; RRID : Addgene_166241

(*Continued on next page*)

Continued

REAGENT or RESOURCE	SOURCE	IDENTIFIER
Software and algorithms		
ZEN lite	Zeiss Microscopy	N/A
Image J	Schneider et al.[7]	https://imagej.nih.gov/ij/
Other		
this work is not part of a clinical trial		

RESOURCE AVAILABILITY

Lead contact

Further information and requests for resources and reagents should be directed to and will be fulfilled by the lead contact, Huan-Huan Shen, (huanhshen@126.com).

Materials availability

This study did not generate new unique reagents.

Data and code availability

All original code has been deposited at https://data.mendeley.com/ and is publicly available as of the date of publication. DOIs are listed in the key resources table.

EXPERIMENTAL MODEL AND STUDY PARTICIPANT DETAILS

Qi-Gui Yan, 52-year-old, male.

Lei Zeng2, 32-year-old, male.

Huan-Huan Shen, 33-year-old, male.

No animal models.

METHOD DETAILS

TRIzol reagent (catalogue number: D9108B), SYBR premix Ex Taq (catalogue number: RR420A) and PrimeScript™ RT reagent Kit with gDNA Eraser (Perfect Real Time) (catalogue number: RR047A) were obtained from TaKaRa Bio Inc. (Otsu, Shiga, Japan); SuperKine™ Maximum Sensitivity Cell Counting Kit-8 (CCK-8) (catalogue number: BMU106-CN) was obtained from Abbkine Scientific (Wuhan, China); oil red O was obtained from (catalogue number: 1320-06-5) Sigma-Aldrich; BODIPY 493/503(catalogue number: 121207-31-6) was obtained from Thermo Fisher Scientific (Waltham, MA,USA); assay kit for free fatty acids (catalogue number: E1001), Tissue Cell Total Cholesterol (TC) Content Enzymatic Determination Kit (catalogue number: E1015-105) and Tissue Cell Triglyceride (TG) Content Enzymatic Determination Kit (catalogue number: E1013-50) were obtained from APPLYGEN (Beijing, China); anti-PRRSV nucleocapsid (N) antibody SDOW17 was obtained from Rural Technologies (WA, USA); anti-FASN antibody (catalogue number: #3180), anti-ACC antibody (catalogue number: #3662), anti-ATGL antibody (catalogue number: 2138S), anti-SQSTOM/P62 antibody (catalogue number: 5114), mouse monoclonal anti-dsRNA antibody (catalogue number: #76651) were obtained from Cell Signaling Technology (Danvers, MA, USA); anti-SMPDL3B antibody (catalogue number: 16552-1-AP) was obtained from Proteintech (Wuhan, China); RIPA Lysis Buffer (strong) (catalogue number: P0013B) was obtained from Beyotime Biotechnology (Zhengzhou China). The reconstituted strains, PRRSV-GFP and 3D4/21-CD163 (generated through lentivirus-mediated overexpression of porcine CD163) were kindly donated by En-Min Zhou from Northwest A&F University (Yangling, Shaanxi, China); Alexa Fluor 488 (catalogue number: A21429), anti-mouse IgG antibody labeled with Alexa Fluor 555 (catalogue number: A21424), and anti-rabbit IgG antibody labeled with Alexa Fluor 488 (catalogue number: A11034) were obtained from Thermo Fisher Scientific (Waltham, MA, USA). The above antibodies were used at a ratio of 1:1000 for immunoblotting and 1:500 for immunofluorescence staining.

Plasmids The coding sequence of porcine SMPDL3B was obtained from porcine lung cDNA and cloned into the p3xFLAG-CMV-14 (Addgene). All plasmids were transfected with Lipofectamine 3000 (Invitrogen, Grand Island, NY).

Cells, viruses, and tissues

HEK293T, 3D4/21-CD163, PAM, and MARC-145 cells were cultured as a monolayer at 37°C under 5% CO_2 with Dulbecco's modified Eagle's medium (DMEM; Gibco, Grand Island, NY), which contained 10% heat inactivated fetal bovine serum (FBS; PAN, Aidenbach, Germany). PAM cells were collected from six-week-old PRRSV-negative pig lungs, and the lungs were aseptically removed after ligating the trachea. The outer surface was washed with 0.9% normal saline, and 30.0 mL PBS was poured into the lungs from the trachea, and the lung surface was gently massaged. The lavage fluid was recovered after 1–2 min and this process was repeated until the lavage fluid was clear. PAM cells were cultured in 1× RPMI1640 medium containing 10% fetal bovine serum, which was supplemented with containing 100 U/mL penicillin and 100 μg/mL streptomycin sulfate. All animal procedures were authorized for experimental animal care and use to comply with animal welfare.

Immunoblot analysis

Whole-cell lysates were prepared in radioimmunoprecipitation assay (RIPA) buffer (50 mM Tris (pH 7.4), 150 mM NaCl, 1% Triton X-100, 1% sodium deoxycholate, 0.1% SDS, sodium orthovanadate, sodium fluoride, EDTA, leupeptin and other inhibitors) supplemented with protease inhibitors (Roche). Protein samples were separated by SDS-PAGE and subsequently transferred to cellulose nitrate membranes. The membrane was incubated in 5% nonfat milk for 1 h and then washed with TBST four times at room temperature for 10 min for the first two times followed by 5 min for the third and fourth times. The membrane was incubated with the primary antibody at 4°C overnight, and then washed four times with TBST at room temperature for 10 min for the first two times followed by 5 min for the third and fourth times. The membrane was then incubated with the second antibody for 1 h at room temperature. The target proteins were detected with the Luminata Crescendo immunoblotting HRP substrate (Millipore, Billerica, MA).

Immunofluorescence assay

The cells were washed in phosphate-buffered saline (PBS) and fixed with 4% paraformaldehyde (PFA) for 30 min at room temperature. The cells were permeabilized in 0.1% Triton X-100 for 5 min and washed three times in PBS, incubated with the primary antibody (1:500) for 1 h, and washed three times in PBS. The cells were incubated with the second antibody (1:1000) for 1 h, then washed three times in PBS and ultra-pure water. Images were acquired using a Zeiss LSM710 confocal microscope. Digital images were obtained using ZEN 2012 software and quantified with ImageJ software.

Quantitative PCR

The total RNA was extracted from cells or supernatants with TRIzol reagent and reverse transcribed into cDNA using a PrimeScript™ RT reagent Kit with gDNA Eraser (Perfect Real Time). The procedure for RNA extraction involves washing cells two times using phosphate-buffered saline, adding 1 mL of TRIzol solution, and lysing the cells until completely detached. Subsequently, adding 0.2 mL of chloroform, shaking the mixture, and allowing it to stand at room temperature. Then centrifuging the mixture and isolating the upper layer for precipitation, followed by adding isopropanol, ethanol, or other appropriate reagents for further washing and precipitation. Finally, drying the RNA using air. qPCR was performed according to the manufacturer's introductions. All reactions were performed in triplicate and the relative amount of mRNAs were calculated with the comparative threshold cycle (CT) method. The results are representative of three independent experiments.

Production of cells stably expressing SMPDL3B shRNA

Short hairpin RNA (shRNA) sequences targeting SMPDL3B were designed using BLOCK-iT RNAi designer (Life Technologies, Carlsbad, CA), the primers shown in Table 1. ShRNA was cloned into the pLKO.1 vector, and 1 μg sh-SMPDL3B, 1.5 μg psPAX2 (packaging-expressing plasmid), and 2 μg pMD2.G (envelope-expressing plasmid) were transfected into human HEK293T cells together and plated on 10-cm dishes for 24 h. After 6 h of transfection, fresh DMEM supplemented with 10% heat-inactivated fetal bovine serum was exchanged and the lentivirus particles were collected after 48 h. MARC-145 and 3D4/21-CD163 cells were infected with lentivirus particles for 36 h, after which MARC-145 cells were selected in medium containing 10 μg/mL puromycin for 1 week and 3D4/21-CD163 cells were selected in medium containing 45 μg/mL puromycin for 10 days. The efficiency of SMPDL3B was detected by qPCR and immunoblotting, the primers shown in Table 1.

Table 1. Primers used for gene cloning and knockdown

Primer	Sequence
sh-SMPDL3B-1	CCGGGGACTACAAGGTATCTCAAGACTCGAGTCTTGAGATACCTTGTAGTCCTTTTTTG
	AATTCAAAAAGGACTACAAGGTATCTCAAGACTCGAGTCTTGAGATACCTTGTAGTCC
sh-SMPDL3B-2	CCGGGCTCATCAGAGAGGTCTTTCCCTCGAGGGAAAGACCTCTCTGATGAGCTTTTTG
	AATTCAAAAAGCTCATCAGAGAGGTCTTTCCCTCGAGGGAAAGACCTCTCTGATGAGC
sh-GPS2-1	CCGGGCCTCGACTCCGGAAGGATTCCTCGAGGAATCCTTCCGGAGTCGAGGCTTTTTG
	AATTCAAAAAGCCTCGACTCCGGAAGGATTCCTCGAGGAATCCTTCCGGAGTCGAGGC
sh-GPS2-2	CCGGGACAGCCTCGACTCCGGAAGGCTCGAGCCTTCCGGAGTCGAGGCTGTCTTTTTG
	AATTCAAAAAGACAGCCTCGACTCCGGAAGGCTCGAGCCTTCCGGAGTCGAGGCTGTC
sh-FGF10-1	CCGGGCTGAAACTCTAGTCCCTTAGCTCGAGCTAAGGGACTAGAGTTTCAGCTTTTTG
	AATTCAAAAAGCTGAAACTCTAGTCCCTTAGCTCGAGCTAAGGGACTAGAGTTTCAGC
sh-FGF10-2	CCGGGCATTTGTCAGCTCACATATACTCGAGTATATGTGAGCTGACAAATGCTTTTTG
	AATTCAAAAAGCATTTGTCAGCTCACATATACTCGAGTATATGTGAGCTGACAAATGC
sh-KCNC2-1	CCGGGCGGGAATAGAAAGGATATGGCTCGAGCCATATCCTTTCTATTCCCGCTTTTTG
	AATTCAAAAAGCGGGAATAGAAAGGATATGGCTCGAGCCATATCCTTTCTATTCCCGC
sh-KCNC2-2	CCGGGGTGATTACACGTGTGCTTCTCTCGAGAGAAGCACACGTGTAATCACCTTTTTG
	AATTCAAAAAGGTGATTACACGTGTGCTTCTCTCGAGAGAAGCACACGTGTAATCACC
sh-MGAT5B-1	CCGGGCTTCTTCTCACTCTGCTTCCCGAAGGAAGCAGAGTGAGAAGAAGCTTTTTG
	AATTCAAAAAGCTTCTTCTCACTCTGCTTCCTTCGGGAAGCAGAGTGAGAAGAAGC
sh-MGAT5B-2	CCGGGGAAGGAGTCTCTAATCTTTACGAATAAAGATTAGAGACTCCTTCCTTTTTG
	AATTCAAAAAGGAAGGAGTCTCTAATCTTTATTCGTAAAGATTAGAGACTCCTTCC
SMPDL3B-sgRNA	AAACTCCACTGAGCTCTTTTGC
Flag-SMPDL3B	CTTGGTCTTTTCAAGCCTCTGT
	CAGGGATGCCACCCGGGATCCTCA GCTTTGGATAAATGG
	AAGGATGACGATGACAAGCTTATG AAAAGTCAGAGGAGC

CRISPR/Cas9-mediated knockout of SMPDL3B in MARC-145 and 3D4/21-CD163 cells

A CRISPR/Cas9 single guide RNA (sgRNA) targeting SMPDL3B was designed, the primers shown in Table 1. SgRNA was cloned into a pLentiCRISPRv2 vector containing a Cas9 expression cassette, after which 1 μg sg-SMPDL3B, 1.5 μg psPAX2 (packaging-expressing plasmid), and 2 μg pMD2.G (envelope-expressing plasmid) were transfected into human HEK293T cells together, and plated on 10 cm dishes for 24 h. After 6 h of transfection, fresh DMEM supplemented with 10% heat-inactivated fetal bovine serum was exchanged and lentivirus particles were collected after 48 h. MARC-145 and 3D4/21-CD163 cells were infected with lentivirus particles for 36 h, after which MARC-145 cells were selected in medium containing 10 μg/mL puromycin for 1 week and 3D4/21-CD163 cells were selected in medium containing 45 μg/mL puromycin for 10 days. The genomic DNA of SMPDL3B deficient cells was extracted and underwent PCR amplification. DNA sequencing was performed to verify the SMPDL3B knockout results. The efficiency of the SMPDL3B knockout was assessed by qPCR and immunoblotting, the primers shown in Table 1.

SMPDL3B-resuce cells

Porcine SMPDL3B was amplified by PCR and cloned into the pLentiCRISPRv2 vector, the primers shown in Table 1. Next, 1 μg of pLentiCRISPRv2-SMPDL3B, 1.5 μg of psPAX2 (packaging-expressing plasmid), and 2 μg of pMD2.G (envelope-expressing plasmid) were transfected into human HEK293T cells. The cells were then plated on 10-cm dishes for 24 h. Packaging of lentivirus particles, screening of SMPDL3B-resuce cells were selected in medium containing 45 μg/mL puromycin for 10 days.

Viral titration

A 50% tissue culture infective dose (TCID50) assay was used to evaluate viral titration. MARC-145 cells were seeded into a 96-well plate with 1×10^4 cells per well and washed three times with PBS after 24 h. Each well

was inoculated with serially 10-fold diluted viruses at 37°C for 1 h, washed three times with PBS, then maintenance fluid (2% FBS–DMEM; 200 μL) was added for 4 days. The TCID50 value was calculated using the Reed-Muench method [93]. All reactions were performed in triplicate.

LD staining

The cells were washed with PBS and fixed in 4% PFA for 30 min at room temperature and washed three times again with PBS. Oil red O staining solution (100 μL, saturated oil red O solution in isopropanol-water at a 3:2 dilution) was added for 15 min. Cells were washed 100 times with double-distilled Millipore water, re-stained with Harris hematoxylin (10 s), washed with PBS, sealed with glycerin gelatin, and observed under a light microscope. The LD number was determined with the ImageJ ''analyze particles'' function (areas of particles of <0.01 mm2 were excluded).

Cells were washed with PBS, fixed in 4% PFA for 30 min at room temperature, washed three times with PBS, and incubated with BODIPY 493/503 (1:500) for 1 h. Digital images were obtained with ZEN 2012 software. Fluorescence intensity was processed using ImageJ software.

Flow cytometry

3D4/21-CD163 and SMPDL3B defective cells were infected with PRRSV-GFP at a multiplicity of infection (MOI) of 10, which was digested with a trypsin-EDTA solution after 36 h of viral infection. The cells were washed twice with precooled PBS, suspended in 0.3 mL precooled PBS, and the GFP-positive cells were detected with a Beckman CytoFLEX flow cytometer. All data were analyzed using CytExpert software.

Determination of intracellular FFAs, TG, and TC

Intracellular FFAs, TC, and TG were assessed with an assay kit for free fatty acids, TC Content Enzymatic Determination Kit and TG Content Enzymatic Determination Kit. According to the manufacturer's instructions of the kits, 3D4/21-CD163 and SMPDL3B defective cells were scraped from the culture plate with a diameter of 10 cm and washed twice with precooled PBS. The cellular lysates were extracted with a syringe needle in 250 μL RIPA buffer and centrifuged at 12,000 × *g* for 10 min at 4°C, then 200 μL of the supernatant was collected to measure the content of FFA, TC, and TG according to the instructions.

QUANTIFICATION AND STATISTICAL ANALYSIS

All data were obtained from at least three independent experiments and analyzed using Prism 8 software (GraphPad Software Inc.) with a two-tailed Student's *t*-test or one-way ANOVA. $P < 0.05$ was considered statistically significant.

Table 1 Primers used for gene cloning and knockdown related to Figures 1C, 5B, and 5E. (Figure 1C The knockdown efficiency of KCNC2, MGAT5B, FGF10, GPS2 and SMPDL3B were detected by RT-qPCR. Figure 5B Immunoblot analysis of SMPDL3B expression in cells from panel A. Figure 5E Immunoblot analysis of SMPDL3B expression in the cells from panel F.).

Table 2 Primers used for RT-qPCR related to Figures 2B, 3A, 3B, 3D, 3E, 4A–4E, 4H, 4M, 4N, 4P, 4R, 5A, 5D, 6A, 6C, 6G, 6H, 7E, and 7F. (Figure 2B RNA was extracted from porcine tissues. Figure 3A The level of SMPDL3B mRNA expression was detected in MARC-145 cells for the indicated time points by RT-qPCR. Figure 3B SMPDL3B mRNA levels were detected in PAM cells for the indicated time points by RT-qPCR. Figure 3D SMPDL3B mRNA levels were detected in MARC-145 cells for the indicated time points by RT-qPCR. Figure 3E The expression of SMPDL3B mRNA was analyzed by RT-qPCR in PRRSV-infected PAM cells at different time points. Figure 4A TNF-α mRNA levels were detected in the cells by RT-qPCR. Figure 4B IL-4 mRNA levels were detected in the cells by RT-qPCR. Figure 4C IL-6 mRNA levels were detected in the cells by RT-qPCR. Figure 4D IL-1β mRNA levels were detected in the cells by RT-qPCR. Figure 4E SMPDL3B mRNA levels in stably expressing sh-SMPDL3B or sh-control cells were detected by RT-qPCR. Figure 4H PRRSV mRNA levels were detected in the cells by RT-qPCR. Figure 4M SMPDL3B mRNA Levels. The levels of SMPDL3B mRNA in stably expressing sh-SMPDL3B or sh-control cells were detected by RT-qPCR. Figure 4N PRRSV mRNA levels. The levels of PRRSV mRNA were detected in cells stably expressing sh-SMPDL3B or sh-control MARC-145 cells infected with PRRSV-JXA1-R (MOI = 0.1) for 48 h using RT-qPCR. Figure 4P SMPDL3B mRNA Levels. Figure 4R PRRSV mRNA levels. Figure 5A PRRSV mRNA levels were detected in cells by RT-qPCR. Figure 5D PRRSV mRNA levels were detected in cells

Table 2. Primers used for RT-qPCR

Primer	Sequence	Product size (bp)
Q-sus-SMPDL3B	CAGCATAGACTTGAGTATCTGGAAA	214
	GGGGACTACCTCTGCGATTC	
Q-sus-FGF10	TGTTGCTGTTCTTGGTGTCTTC	179
	AGAGAATAGCTTTCTCCAGCGG	
Q-sus-GPS2	GGAACAAATCCTGAAGTTGCAGG	195
	ATGCTGAGGAGGTGAGTTCCT	
Q-sus-MGAT5B	TGCTTCTGCACAGCAAGGTG	196
	CAAAACCACTCGACCTCACTG	
Q-sus-KCNC2	TTCTTCTTCGACCGGCACCC	208
	TCTCGAAGATGTCGAGCGCC	
Q-sus-GADPH	AAGTTCCACGGCACAGTCAA	161
	GCCTTCTCCATGGTCGTGAA	
Q-sus-β-actin	CTGAACCCCAAAGCCAACCGT	317
	TTCTCCTTGATGTCCCGCACG	
Q-Chlorocebus-β-actin	CGTGGACATCCGTAAAGAC	182
	GGAAGGTGGACAGCGAGGC	
Q-PRRSV ORF7	AAACCAGTCCAGAGGCAAGG	222
	GCAAACTAAACTCCACAGTGTAA	
Q-sus-ACC1	GGAGACAAACAGGGACCATTACA	144
	CAGGGACTGCCGAAACATC	
Q-sus-FASN	TGCTCCTGCACGTCTCCC	240
	CTGCTGAAGCCTAACTCCTCG	
Q-sus-SCD	AATGGAGGGGGCAAGTTGGA	196
	GGTGGGGATCAATATGATCCC	
Q-sus-ATGL	TGTGGCCTCATTCCTCCTAC	271
	TCGTGGATGTTGGTGGAGCT	
Q-sus-HSL	TCAGGTGTCTTTGCGGGTAT	213
	CTTGTGCGGAAGAAGATGCT	
Q-sus-MGL	GTCTTCCTTCTGGGCCATCTC	157
	GTTGAGCACTTTCGCAGCAA	
Q-sus- IL-1β	ATGGCTTACTACAGCGGCAA	306
	ACAAGCGTCGTTATTGCGTG	
Q-sus-IL-6	CGGATGCTTCCAATCTGGGT	355
	CAGGTGCCCCAGCTACATTA	
Q-sus-IL-8	AAAACCCATTCTCCGTGGCT	352
	AGGTGCAAGTTGAGGCAAGA	
Q-sus-TNF-α	CTGTAGGTTGCTCCCACCTG	176
	CCAGTAGGGCGGTTACAGAC	

by RT-qPCR. Figure 6A RT-qPCR analysis was performed to determine the number of PRRSV particles on the surface of stably expressing sh-SMPDL3B or sh-control cells. Figure 6C RT-qPCR analysis of PRRSV numbers in stably expressing sh-SMPDL3B or sh-control cells. Figure 6G The efficiency of viral assembly was determined by the ratio of the virus titer in the supernatant to the total PRRSV genome. Figure 6H The efficiency of viral secretion was determined by the ratio of intra- and extracellular infectivity relative to total infectivity. Figure 7E Levels of ACC1, FASN, and SCD were detected by RT-qPCR. Figure 7F Levels of ATGL, HSL, and MGL mRNA expression were detected by RT-qPCR.).